J. Fluid Mech. (1992), *vol.* 240, *pp.* 259–288
Printed in Great Britain

Insoluble surfactant spreading on a thin viscous film: shock evolution and film rupture

By O. E. JENSEN[1] AND J. B. GROTBERG[1,2]

[1] Department of Biomedical Engineering, Northwestern University, Evanston, IL 60208, USA
[2] Department of Anesthesia, Northwestern University Medical School, Chicago, IL 60611, USA

(Received 27 June 1991)

Lubrication theory and similarity methods are used to determine the spreading rate of a localized monolayer of insoluble surfactant on the surface of a thin viscous film, in the limit of weak capillarity and weak surface diffusion. If the total mass of surfactant increases as t^α, then at early times, when spreading is driven predominantly by Marangoni forces, a planar (axisymmetric) region of surfactant is shown to spread as $t^{(1+\alpha)/3}$ ($t^{(1+\alpha)/4}$). A shock exists at the leading edge of the monolayer; asymptotic methods are used to show that a wavetrain due to capillary forces exists ahead of the shock at small times, but that after a finite time it is swamped by diffusive effects. For $\alpha < \frac{1}{2}$ ($\alpha < 1$), the diffusive lengthscale at the shock grows faster than the length of the monolayer, ultimately destroying the shock; subsequently, spreading is driven by diffusion, and proceeds as $t^{\frac{1}{2}}$. The asymptotic results are shown to be good approximations of numerical solutions of the governing partial differential equations in the appropriate limits. Additional forces are also considered: weak vertical gravity can also destroy the shock in finite time, while effects usually neglected from lubrication theory are important only early in spreading. Experiments have shown that the severe thinning of the film behind the shock can cause it to rupture: the dryout process is modelled by introducing van der Waals forces.

1. Introduction

One reason that many prematurely born infants develop respiratory distress syndrome (RDS) is that their lungs are not sufficiently mature to produce adequate quantities of pulmonary surfactant. This substance plays a vital role in reducing the surface tension of the liquid which lines alveoli and lung airways, and its deficiency can give rise to respiratory difficulties associated with airway closure, decreased lung compliance, pulmonary oedema and mechanical damage of the airway linings (Robertson 1984), often with fatal consequences. An effective technique for the treatment of this condition (and of adult RDS) is to deliver surfactant externally, either directly through an endotracheal tube, or through inhalation of surfactant in aerosol form (Shapiro 1989). Since the barrier between pulmonary capillaries and the liquid layer in alveoli is so thin, aerosol inhalation is also used as a method of rapid drug delivery. In order to improve our understanding of these techniques, we examine one element of the delivery process, the spreading of localized, insoluble surfactant on a thin, viscous layer of fluid.

When a drop of surfactant comes into contact with a clean liquid substrate, the

large surface tension difference at its edge, expressed by the positive value of the spreading coefficient

$$\tilde{S} = \sigma_0 - \sigma_m, \tag{1.1}$$

causes it to spread. In (1.1) σ_m represents the combined surface tensions of the drop/substrate and drop/gas boundaries and σ_0 the higher surface tension of the substrate/gas boundary. Spreading is achieved through the development, ahead of the bulk of the drop, of a thin monomolecular layer of surfactant on the surface of the substrate, along which the jump in surface tension $\tilde{S}$ is accommodated (DiPietro, Huh & Cox 1978). The concentration of surfactant in this monolayer increases from zero at its leading edge to Γ_m (the critical micelle concentration) where the monolayer meets the bulk of the drop. The surface tension σ^* at each point along the monolayer is related to the local surfactant concentration Γ^* through an empirically determined equation of state $\sigma(\Gamma^*/\Gamma_m)$, such that $\sigma(0) = 1$, $\sigma(1) = 0$ and

$$\sigma^* = \sigma_m + \tilde{S}\sigma(\Gamma^*/\Gamma_m). \tag{1.2}$$

The gradient in Γ^*, and thus in σ^*, along the monolayer induces a shear stress at the surface of the underlying liquid, and thus a Marangoni flow in the substrate. If the liquid substrate is thin, and if diffusion of the surfactant on the surface of the film is sufficiently slow, the flow induces large deformations in the film (Borgas & Grotberg 1988; Gaver & Grotberg 1990; referred to respectively as BG and GG1 hereinafter.). The leading edge of the monolayer behaves like an advancing rigid plate, and the abrupt transition to undisturbed conditions just ahead of the monolayer produces a shock-like discontinuity in film height, with the film elevated beneath the leading edge of the monolayer to almost twice its undisturbed height. To accommodate this elevation the film thins in regions closer to the centre of the drop (GG1). Gaver & Grotberg (1992, hereinafter referred to as GG2) observed experimentally that if the initial gradients in surface tension are sufficiently large, the deformation of the film induced by the spreading of a surfactant droplet may be severe enough for the thinnest part of the film to rupture, leaving a dry ring.

Of particular importance in the context of surfactant replacement therapy are estimates of spreading rates, either of a planar front of surfactant advancing along the mucus lining of an airway, or of a droplet of surfactant spreading over the film covering an alveolar wall. In both cases, the substrate film is thin enough for gravitational effects to be negligible. In most experimental measurements of spreading rates, however, thicker substrates were used for which gravity was significant. Ahmad & Hansen (1972) examined a spreading strip of surfactant, and observed spreading proportional to $t^{\frac{1}{2}}$; they accounted for this with an *ad hoc* model that neglected gravitational effects (among others). GG2, who examined spreading drops, could not identify a universal spreading rate, but could describe their experimental results using a model developed using lubrication theory. In a separate numerical study using this model, GG1 predicted that the spreading rate of a drop was approximately $t^{0.25}$ when gravity and surface diffusivity were weak, increasing to $t^{0.35} - t^{0.45}$ when diffusion was stronger. A theoretical estimate of spreading rate was given by BG, who studied the steady advance of a monolayer pushed along by a barrier, and thereby predicted that if surfactant is supplied to the monolayer at a rate of $t^{\frac{1}{2}}$, a planar front advances at a rate of $t^{\frac{1}{2}}$. This result was not directly related to the time-dependent governing equations, however.

In modelling the spreading process, much can be learned by considering the spreading of an insoluble surfactant monolayer on a thin film, neglecting the

behaviour of the bulk surfactant droplet at the upstream edge of the monolayer. (We will therefore not be considering the fingering instability at the edge of the bulk droplet observed experimentally by Troian, Wu & Safran (1989) and modelled by Troian, Herbolzheimer & Safran (1990); nor do we consider the effects of solubility, discussed by Halpern & Grotberg (1991).) Using lubrication theory, two coupled nonlinear evolution equations for the film thickness and the surfactant concentration distribution can be derived (BG, GG1, §2). BG studied such equations in a steadily translating frame, representing an advancing planar front, and showed how surface diffusion of the surfactant can smooth the shock at the leading edge of the monolayer. GG1 computed time-dependent solutions of these equations in an axisymmetric geometry, to describe the evolution of a disk-like monolayer of surfactant. They examined the effects of a vertical gravitational field, and showed how a backflow due to hydrostatic pressure gradients may be generated by the large gradients in film height.

In this paper we consider two additional effects: the mean surface tension of the liquid film (which we shall refer to below as 'capillarity'); and long-range intermolecular forces (van der Waals forces). Although capillarity is a weak force, it has a significant qualitative effect on the structure of the shock (Espinosa 1991). It is also important in stabilizing the film against instabilities due to van der Waals forces. These forces, too, are very weak, unless the film becomes extremely thin (less than 1000 Å), in which case they encourage depressions in the film to grow, and may ultimately cause the film to rupture (Ruckenstein & Jain 1974; Williams & Davis 1982). Since film rupture has such a dramatic effect on the spreading process, it interferes severely with methods of delivery of surfactant or drugs, making it of considerable importance to establish the conditions under which rupture can occur. We will consider below a potential mechanism for the dryout seen experimentally, namely that the severe thinning due to Marangoni effects is sufficient to induce a rupture instability.

We begin, however, by presenting a class of similarity solutions of the reduced evolution equations, in which there is a balance of viscous and Marangoni forces alone (§3). The spreading rates of these solutions depend both on the geometry of the problem, and on the rate at which surfactant is supplied to the monolayer: an axisymmetric drop is predicted to spread at a rate of $t^{\frac{1}{4}}$; a planar strip at a rate of $t^{\frac{1}{3}}$; and a planar front at a rate of $t^{\frac{1}{2}}$. These predictions correspond to results recently obtained by Espinosa (1991). In §4 these solutions are compared to numerical solutions of the evolution equations that are additionally subject to the effects of weak capillarity and weak surface diffusion of surfactant. It is confirmed that the spreading rates predicted by the similarity solutions are useful and accurate approximations, but only over certain time intervals. In order to quantify these times, the asymptotic structure of the shock is investigated in §5. The role of gravity, of an existing weak concentration of surfactant on the film ahead of the shock, and of some additional forces normally neglected in the lubrication approximation are also examined. We show that for a spreading drop or strip on an uncontaminated film, the shock will be destroyed in finite time by either gravitational or diffusive forces. Thereafter, the spreading rate changes: if diffusion is the dominant force, for example, it is shown in §6 that the spreading rate of a drop or a strip becomes $t^{\frac{1}{2}}$.

In §7 we investigate the conditions under which the rapid spreading of a drop of surfactant can induce the film to rupture. It will be demonstrated that Marangoni forces alone are not sufficient to induce the film thickness to reach zero in finite time, but that they deform the film sufficiently to allow van der Waals forces to overcome

the stabilizing effects of capillarity (and of the surfactant monolayer itself) and give rise to dryout. Section 8 contains a discussion of the results.

2. The model

The model to be investigated here has been described in detail previously by GG1 and so only a brief summary is given. We will consider a thin, planar film of a viscous, incompressible, Newtonian fluid lying on a horizontal plane and having a monolayer of insoluble surfactant at its upper surface.

The variables of the flow are scaled as follows. Let $\tilde{U}$ be a typical horizontal velocity, $\tilde{H}$ the undisturbed height of the film, $\tilde{L}$ the initial horizontal length of the monolayer, and $\tilde{S}/\tilde{L}$ (see (1.1)) the scale of the surface tension gradients. Since it is the tangential stress boundary condition that drives Marangoni flow (see (2.11) below), we set $\mu\tilde{U}/\tilde{H} = \tilde{S}/\tilde{L}$, where μ is the fluid's dynamic viscosity. By imposing the condition that $\epsilon = \tilde{H}/\tilde{L} \ll 1$, lubrication theory may be used. Thus we choose to scale the vertical velocity by $\epsilon\tilde{U}$, time by $\tilde{H}/\epsilon\tilde{U}$ and the pressure by $\mu\tilde{U}\tilde{L}/\tilde{H}^2 \equiv \tilde{S}/\tilde{H}$. We suppose that the Reynolds number $Re = \rho\tilde{U}\tilde{L}/\mu$ is sufficiently small that the leading-order inertial terms in the momentum equation, of $O(\epsilon^2 Re)$, are negligible.

The surfactant concentration in the monolayer is scaled so that $\Gamma = \Gamma^*/\Gamma_m$. We scale the surface tension σ^* of the film so that (1.2) becomes

$$\sigma^* = \tilde{S}\left(\frac{\mathscr{S}}{\epsilon^2} + \sigma(\Gamma)\right), \tag{2.1}$$

where $\mathscr{S} = \epsilon^2\sigma_m/\tilde{S}$. This ensures that capillary effects due to the constant component of σ^*, $\mathscr{S}/\epsilon^2$, arise at the same order as Marangoni effects due to spatial gradients of the component $\sigma(\Gamma)$, but that the two effects are uncoupled at leading order in ϵ. The equation of state $\sigma(\Gamma)$ is in general nonlinear: although a linear law will be used predominantly below, this model allows the use of a nonlinear relation, such as one related to that used by GG1,

$$\sigma(\Gamma) = (\beta+1)\,[1+\theta(\beta)\,\Gamma]^{-3} - \beta, \tag{2.2}$$

$$\theta(\beta) = \left(\frac{\beta+1}{\beta}\right)^{\frac{1}{3}} - 1. \tag{2.3}$$

β relates to the 'activity' of the surfactant, i.e. to the nonlinearity of (2.2), as shown in figure 8(*b*) below; unlike GG1, we allow $\mathscr{S}$ to be independent of β.

In the following, all variables are non-dimensionalized by the above scalings, and for brevity all $O(\epsilon^2)$ quantities will be neglected. Both axisymmetric and planar distributions of surfactant will be of interest in later sections, and so we use a notation that accommodates both geometries. Taking coordinates (x, z), with z vertical, we allow x to represent either a horizontal or radial coordinate. The corresponding velocity field is $(u(x,z,t), w(x,z,t))$. The film surface is at $z = h(x,t)$. We define $\bar{\partial}_x h \equiv h_x$ in a planar geometry, and $\bar{\partial}_x h \equiv x^{-1}(xh)_x$ in an axisymmetric geometry.

The equations of mass and momentum conservation for the film are

$$\bar{\partial}_x u + w_z = 0, \tag{2.4}$$

$$0 = -p_x - \phi_x + u_{zz}, \tag{2.5}$$

$$0 = -p_z - \phi_z - \mathscr{G}, \tag{2.6}$$

where $\mathscr{G} = \rho g\tilde{H}^2/\tilde{S}$ is a parameter representing a gravitational force directed vertically downwards when $\mathscr{G} > 0$, p is the pressure and ϕ is a potential energy per

unit volume in the liquid representing the effects of van der Waals forces. Following Ruckenstein & Jain (1974), we assume

$$\phi(x,t) = \frac{\mathscr{A}}{h^3}. \tag{2.7}$$

$\mathscr{A}$ is related to the Hamaker constant $\tilde{A}$ by $\mathscr{A} = \tilde{A}/(6\pi\tilde{S}\tilde{H}^2)$. Other types of intermolecular force will be not considered.

The boundary conditions for the flow are as follows. A no-slip condition

$$u = w = 0 \tag{2.8}$$

is imposed at $z = 0$. Using (2.4), the kinematic boundary condition at $z = h$ may be expressed as

$$h_t + \bar{\partial}_x\left(\int_0^h u\,\mathrm{d}z\right) = 0. \tag{2.9}$$

The normal and tangential stress conditions at $z = h$ are

$$p(x, z = h-, t) = -\mathscr{S}\bar{\partial}_x(h_x) \tag{2.10}$$

(assuming $p = 0$ above the film) and

$$u_z = \sigma_x. \tag{2.11}$$

The surfactant conservation relation is

$$\Gamma_t + \bar{\partial}_x(u_s\Gamma) = \mathscr{D}\bar{\partial}_x(\Gamma_x). \tag{2.12}$$

$\Gamma(x,t)$ varies through advection ($u_s = u(x, z = h, t)$) and surface diffusion ($\mathscr{D}^{-1} \equiv \tilde{U}\tilde{H}/\epsilon\tilde{D}$ is the surface Péclet number, where $\tilde{D}$ is the surface diffusivity of surfactant, assumed constant).

Equations (2.6) and (2.10) show that

$$p(x,z,t) = \mathscr{G}(h-z) - \mathscr{S}\bar{\partial}_x(h_x). \tag{2.13}$$

Since p_x and ϕ_x are independent of z, (2.5) may be integrated straightforwardly, using boundary conditions (2.8) and (2.11), to give

$$u = \tfrac{1}{2}(p_x + \phi_x)(z^2 - 2zh) + \sigma_x z. \tag{2.14}$$

When this is incorporated into the kinematic boundary condition (2.9) and the surfactant conservation relation (2.12), we get

$$h_t + \tfrac{1}{2}\bar{\partial}_x(h^2\sigma_x) - \tfrac{1}{3}\mathscr{G}\bar{\partial}_x(h^3h_x) + \tfrac{1}{3}\mathscr{S}\bar{\partial}_x\{h^3[\bar{\partial}_x(h_x)]_x\} + \mathscr{A}\bar{\partial}_x(h^{-1}h_x) = 0, \tag{2.15a}$$

$$\Gamma_t + \bar{\partial}_x(\Gamma h\sigma_x) - \tfrac{1}{2}\mathscr{G}\bar{\partial}_x(\Gamma h^2h_x) + \tfrac{1}{2}\mathscr{S}\bar{\partial}_x\{\Gamma h^2[\bar{\partial}_x(h_x)]_x\} + \tfrac{3}{2}\mathscr{A}\bar{\partial}_x(\Gamma h^{-2}h_x) = \mathscr{D}\bar{\partial}_x(\Gamma_x). \tag{2.15b}$$

These equations are coupled by the surfactant equation of state (2.2). Note that in practice it is highly unlikely that gravitational and intermolecular forces would ever be of the same order, so we shall not consider situations in which both $\mathscr{A}$ and $\mathscr{G}$ appear together.

3. Similarity solutions

In this section it is shown that a simple form of (2.15), in which there is a balance of viscous and Marangoni forces alone (i.e. $\mathscr{G} = \mathscr{S} = \mathscr{A} = \mathscr{D} = 0$), possesses a set of similarity solutions describing the spreading of a region of localized surfactant. Three distributions of surfactant will be of particular interest in what follows: a planar

strip; an axisymmetric drop; and a planar front, behind which surfactant is supplied at a given rate. For convenience we shall refer to these cases simply as strip, drop and front in what follows.

We shall suppose that the total mass of surfactant in $x > 0$, which in planar or axisymmetric geometry is respectively

$$M = \int_0^\infty \Gamma \,\mathrm{d}x, \quad \text{or} \quad M = 2\pi \int_0^\infty x\Gamma \,\mathrm{d}x, \tag{3.1a, b}$$

may be expressed as

$$M = Qt^\alpha. \tag{3.2}$$

Thus a strip or a drop is represented by $\alpha = 0$ and a front by some $\alpha > 0$. In deriving similarity solutions we will take advantage of the fact that Q must be an invariant of (2.15b).

For the strip or the drop, the surfactant spreads out rapidly enough for Γ to become everywhere quite small, even after moderate times. Accordingly the significance of the nonlinearity of the equation of state (2.2) diminishes, so that σ_x in (2.15) can be replaced by $-E\Gamma_x$, where $E = -\mathrm{d}\sigma/\mathrm{d}\Gamma(\Gamma = 0)$. E may be set to unity by the transformation $\Gamma \to E\Gamma$. We will therefore take $E = 1$ in what follows; this is equivalent to considering the limit $\beta \to \infty$ in (2.2).

When simplified as described above, (2.15) reduces to

$$h_t - \tfrac{1}{2}\bar{\partial}_x(h^2\Gamma_x) = 0, \quad \Gamma_t - \bar{\partial}_x(\Gamma h \Gamma_x) = 0. \tag{3.3a, b}$$

Writing $h(x,t) = H_0(\xi), \Gamma(x,t) = G_0(\xi)/t^b$ and $\xi = x/t^a$, (3.3) becomes independent of t only if $2a+b = 1$. Balancing powers of t in (3.1) and (3.2) gives $a-b = \alpha$ or $2a-b = \alpha$ in planar or axisymmetric geometries respectively. Thus we have in planar geometry

$$a = \tfrac{1}{3}(1+\alpha), \quad b = \tfrac{1}{3}(1-2\alpha), \tag{3.4a}$$

and in axisymmetric geometry

$$a = \tfrac{1}{4}(1+\alpha), \quad b = \tfrac{1}{2}(1-\alpha). \tag{3.4b}$$

This suggests that a planar strip spreads like $t^{\frac{1}{3}}$, while an axisymmetric drop spreads like $t^{\frac{1}{4}}$. A range of values of α are potentially appropriate for a spreading planar front: $0 < \alpha \leqslant \frac{1}{2}$. (Note that we must have $b \geqslant 0$, since if b were negative, Γ would grow without bound as t increases; Γ must remain less than unity for a monolayer not to form a micelle.) $\alpha = \frac{1}{2}$, for which $b = 0$, is of interest as a limiting case (incidentally, it allows the use of a nonlinear equation of state), and we shall consider it when discussing a planar front. We note that it is consistent with the prediction of BG: when surfactant is supplied to the monolayer at a rate of $t^{\frac{1}{2}}$, the monolayer advances at the same rate.

We shall be interested in later sections in solutions of (2.15) (including the effects of weak diffusivity, etc.) having a shock-like structure at the leading edge of the advancing monolayer, with $h = 1, \Gamma = 0$ ahead of the shock. The shock's position will be determined by the total mass of surfactant, and so we scale coordinates using Q to put the shock at $\xi = 1$. The formal transformation that we shall consider is therefore

$$h(x,t) = H(\xi,\tau), \quad \Gamma(x,t) = \frac{\xi_s^2 G(\xi,\tau)}{t^b}, \quad \xi = \frac{x}{\xi_s t^a}, \quad \tau = t, \tag{3.5}$$

so that the location of the shock in the original coordinates is given by $x_s = \xi_s(Q)t^a$. From (3.1), we have

$$\xi_s = \left(\frac{Q}{\int_0^\infty G\,\mathrm{d}\xi}\right)^{\frac{1}{3}} \quad \text{or} \quad \xi_s = \left(\frac{Q}{2\pi\int_0^\infty \xi G\,\mathrm{d}\xi}\right)^{\frac{1}{4}} \tag{3.6a, b}$$

in planar or axisymmetric geometries respectively. Equation (2.15) transforms to

$$\tau H_\tau = a\xi H_\xi + \tfrac{1}{2}\bar{\partial}_\xi(H^2 G_\xi) + \left(\frac{\mathscr{G}\tau^b}{3\xi_s^2}\right)\bar{\partial}_\xi(H^3 H_\xi) - \left(\frac{\mathscr{S}}{3\xi_s^4\tau^{4a-1}}\right)\bar{\partial}_\xi\{H^3[\bar{\partial}_\xi(H_\xi)]_\xi\} - \left(\frac{\mathscr{A}\tau^b}{\xi_s^2}\right)\bar{\partial}_\xi(H^{-1}H_\xi) \tag{3.7a}$$

$$\tau G_\tau = a\xi G_\xi + bG + \bar{\partial}_\xi(GHG_\xi) + \left(\frac{\mathscr{G}\tau^b}{2\xi_s^2}\right)\bar{\partial}_\xi(GH^2H_\xi) - \left(\frac{\mathscr{S}}{2\xi_s^4\tau^{4a-1}}\right)\bar{\partial}_\xi\{GH^2[\bar{\partial}_\xi(H_\xi)]_\xi\} - \left(\frac{3\mathscr{A}\tau^b}{2\xi_s^2}\right)\bar{\partial}_\xi(GH^{-2}H_\xi) + \left(\frac{\mathscr{D}\tau^b}{\xi_s^2}\right)\bar{\partial}_\xi(G_\xi). \tag{3.7b}$$

We return now to the case in which $\mathscr{G} = \mathscr{S} = \mathscr{A} = \mathscr{D} = 0$, and seek fixed points of the above equations, with $H = H_0(\xi)$ and $G = G_0(\xi)$. They are solutions of

$$a\xi H_{0\xi} + \tfrac{1}{2}\bar{\partial}_\xi(H_0^2 G_{0\xi}) = 0, \tag{3.8a}$$

$$a\xi G_{0\xi} + bG_0 + \bar{\partial}_\xi(G_0 H_0 G_{0\xi}) = 0, \tag{3.8b}$$

with boundary conditions $H_0 = 1$, $G_0 = 0$, for $\xi > 1$. We seek solutions with a shock at $\xi = 1$, having discontinuities in H_0 and $G_{0\xi}$: integrating (3.8) across $\xi = 1$ it is straightforward to show that upstream of the shock we must have

$$H_0(\xi = 1-) = 2, \quad G_{0\xi}(\xi = 1-) = -\tfrac{1}{2}a. \tag{3.9}$$

These conditions guarantee that the speed of the shock, $\dot{x}_s$, equals the surface velocity of the film at the shock, $-\Gamma_x h$, so that there is no transport of surfactant ahead of the shock. The tip of the monolayer acts as an advancing rigid plate, and the discontinuity in film height is an adjustment to the free-surface boundary condition ahead of the shock. Fortunately when $a = 0$, (3.8) can be integrated exactly to give, for $0 < \xi < 1$,

$$H_0 = 2\xi, \quad G_0 = \tfrac{1}{6}(1-\xi) \quad \text{(strip)}, \tag{3.10a}$$

$$H_0 = 2\xi^2, \quad G_0 = -\tfrac{1}{8}\log\xi \quad \text{(drop)}. \tag{3.10b}$$

Transforming back to (x, t) coordinates, we can replace $\int_0^\infty G\mathrm{d}\xi$ in (3.6) by $\int_0^1 G_0\mathrm{d}\xi$ to determine ξ_s, from which it follows that

$$x_s = (12Qt)^{\frac{1}{3}} \text{ (strip)}, \quad x_s = \left(\frac{16Qt}{\pi}\right)^{\frac{1}{4}} \text{ (drop)}. \tag{3.11a, b}$$

Figure 1 shows these similarity solutions for the strip, the drop and the front. The frontal solution was determined numerically from (3.8); in this case we cannot replace the integral in (3.6*a*) by $\int_0^1 G_0\,\mathrm{d}\xi$ because the latter does not converge. (We remark here that similar solutions with both G_0 and $G_{0\xi}$ discontinuous at $\xi = 1$ can be found, e.g. $G = G_s + \frac{1}{6}(1-\xi)$ in (3.10*a*) where G_s is a constant. Numerical results indicate, however, that in the presence of diffusion the solutions with $G_s > 0$ are unstable. We shall therefore assume that G is everywhere continuous.)

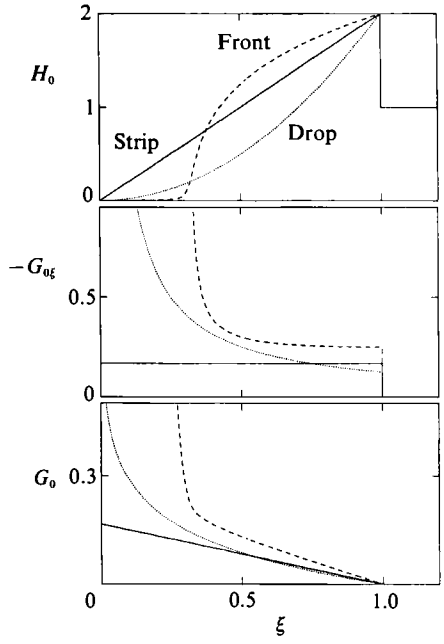

FIGURE 1. Similarity solutions (3.10*a*) representing a spreading planar strip (——, spreading as $t^{\frac{1}{3}}$) an axisymmetric drop (3.10*b*) (..., $t^{\frac{1}{4}}$) and a planar front (– – –, $t^{\frac{1}{5}}$). The film height H_0, scaled surface shear stress $-G_{0\xi}$ and scaled surfactant distribution G_0 are plotted as functions of ξ.

The similarity solutions shown in figure 1 display a number of important features of surfactant spreading. They describe how, as the monolayer advances, the gradient in surfactant concentration across the monolayer diminishes in magnitude, reducing the shear stress that drives the spreading, so that the rate of advance diminishes. The solutions are inaccurate in a number of respects, however. They are obviously physically invalid near $\xi = 0$, since one cannot have zero H and (in general) infinite G at this point. We will see in §4 that in practice there is always a zone at $\xi = 0$ across which the solution adjusts to physically realizable boundary conditions. The solutions also contain shocks, contravening the assumptions underlying lubrication theory. When additional effects such as surface diffusion are included, however, the large gradients will be reduced and this difficulty will no longer be significant.

4. Comparison with numerical solutions

Having established the existence of some exact solutions of a simplified form of (2.15), we now determine the conditions under which these resemble those solutions of (2.15) that satisfy physically realistic boundary conditions and that are subject to weak diffusive and capillary forces. These full solutions have been obtained *numerically* by the method of lines, using second-order finite differences in space and Gear's method in time. The numerical scheme was developed from that used by Halpern & Grotberg (1991). The number of grid points used in the computations varied between $N = 101$ and $N = 301$.

Rather than solve (2.15), it was more efficient to compute solutions of (3.7) in transformed coordinates (ξ, τ). We will follow the transformation of (3.5), but without using the normalization of ξ and Γ: this is equivalent to setting $\xi_s = 1$ in (3.5) and (3.7). We shall again consider three cases, to be presented in turn below, the

spreading of a strip, a drop and a front. The boundary conditions used in the computations were chosen as follows. Far downstream, the film is undisturbed, i.e. $H(\xi,\tau)=1, G(\xi,\tau)=0$. The boundary condition upstream is determined by considering the total mass of surfactant (3.1), which for a planar geometry is $Q=\int_0^\infty G\,\mathrm{d}\xi$. Recall that Q must be an invariant of (3.7*b*), i.e. $Q_\tau=0$. Integrating (3.7*b*) by parts, we find that this condition requires that, in a planar geometry,

$$G_\xi(0,\tau)=\frac{-\alpha Q}{(G(0,\tau)H(0,\tau)+\mathscr{D}\tau^b)}. \tag{4.1}$$

Thus to model the spreading of a strip ($\alpha=0$), we set $G_\xi=0$ at $\xi=0$, as one would expect. The same condition is appropriate for a drop. For planar frontal spreading we set $\alpha=\frac{1}{2}$ in (4.1). The boundary conditions on H at $\xi=0$ are that $H_\xi=H_{\xi\xi\xi}=0$.

Integration was begun at $\tau=1$, starting with a uniform film ($H=1$) and an arbitrary distribution of surfactant. For the strip and drop computations the following distribution was chosen:

$$G(\xi,1)=\tfrac{1}{2}G_a\left[1-\tanh\left(\frac{\xi-\xi_0}{\xi_w}\right)\right]. \tag{4.2}$$

For the front calculation, the initial surfactant distribution was

$$G(\xi,1)=(\tfrac{1}{2}\xi_w^2-\mathscr{D})\exp(-\xi/\xi_w). \tag{4.3}$$

4.1 *Planar strip*

Figure 2(*a*) shows the evolution of film height and surfactant distribution from an initial condition (4.2) for which $G_a=1$, $\xi_0=0.5$ and $\xi_w=0.1$. The predicted position of the shock was determined from (3.11*a*), and the corresponding similarity solution is shown as a dotted line. The parameters used in the computation were $\mathscr{D}=0.002$, $\mathscr{S}=10^{-4}$, $\mathscr{G}=\mathscr{A}=0$ and $\beta=100$.

As the strip of surfactant begins to spread, there is a welling of the film behind the leading edge of the monolayer, and a corresponding decrease of film height further behind this. As the elevation in film height grows, a shock-like structure develops in H and in the surface shear stress $-G_\xi$. H becomes linear in ξ, parallel to the similarity solution, over a growing part of its range behind the shock; at the same time $-G_\xi$ flattens across a similar range. The shocks in H and $-G_\xi$ are smoothed by both weak diffusive and capillary forces. The effect of cappilarity is demonstrated by the weak train of waves ahead of the advancing monolayer, and the narrow, decaying peak in $-G_\xi$ just behind the shock.

Figure 2(*b*) shows the subsequent evolution of the solution. Across much of the monolayer the computed solution lies very close to the similarity solution. There are obvious discrepancies, however, near $\xi=0$, where there is a boundary layer across which the upstream boundary conditions $H_\xi=G_\xi=0$ are accommodated, and at the shock. The upstream boundary layer decreases in size as time increases, and a growing proportion of the solution in this region approaches the similarity state. Note that the shear stress $-G_\xi$ has a maximum value very close to the point at which the film is thinnest: viscous and Marangoni forces are dominant in this region, and a large surface shear stress is necessary to transport surfactant downstream where viscous stresses are greatest. At the shock, the lengthscale and magnitude of the wavetrain diminish as time increases, until the waves ultimately disappear; likewise, the peak in $-G_\xi$ vanishes also. As the shock advances and slows, the region over which diffusion smooths H and $-G_\xi$ broadens gradually, and the maximum film height falls as a result.

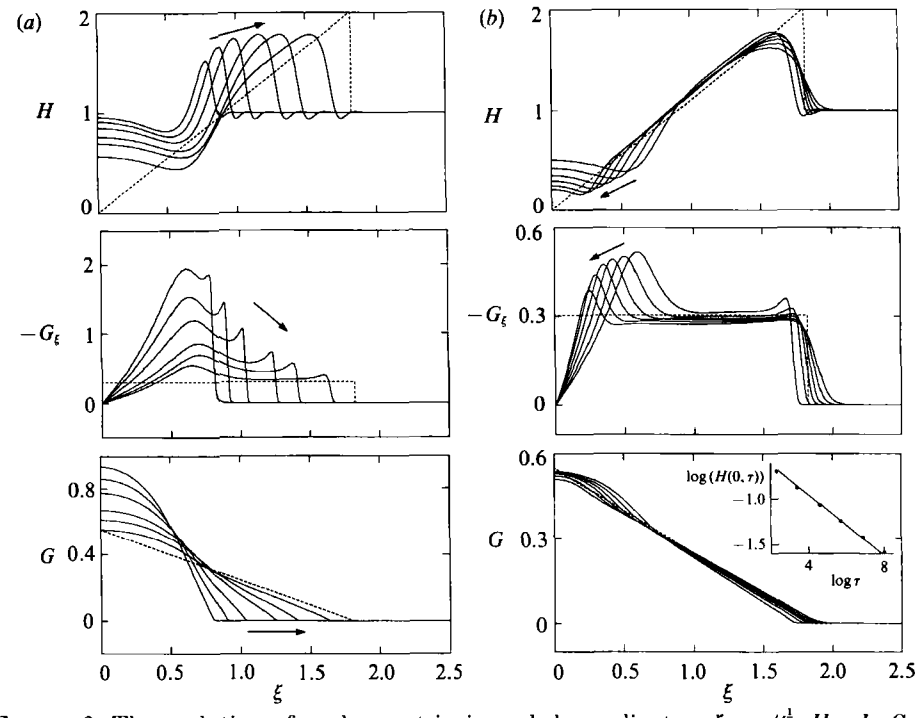

FIGURE 2. The evolution of a planar strip in scaled coordinates: $\xi = x/t^{\frac{1}{3}}$, $H = h$, $G = t^{\frac{1}{3}}\Gamma$ and $G_\xi = t^{\frac{2}{3}}\Gamma_x$. (*a*) shows the transient behaviour at times 1.05, 1.1, 1.2, 1.5, 2.0, 5.0; the dotted line shows the corresponding similarity solution. (*b*) shows the subsequent development of the solution, at times 10, 30, 100, 300, 1000, 3000. Arrows indicate increasing time. Parameter values are $\mathscr{D} = 0.002$, $\mathscr{G} = 0$, $\mathscr{S} = 10^{-4}$, $\mathscr{A} = 0$, $\beta = 100$, $N = 301$. The inset on the lowest panel of (*b*) shows $\log(H(0,\tau))$ as a function of $\log\tau$; the straight line has a slope of $-\frac{1}{6}$.

The rate of decay of the upstream boundary layer can be estimated as follows. We observe first of all that $H(0,\tau)$, $H_{\min}(\xi,\tau)$ and $-(G_\xi)_{\max}(\xi,\tau)$ all change considerably more rapidly than the surfactant distribution $G(\xi,\tau)$. It is clear also that the evolving boundary layer (at least for H and G_ξ) has a self-similar structure. To see how to exploit these features we consider the governing equations (3.7), (the effects of capillarity and diffusion may be neglected from a leading-order approximation in this region)

$$\tau H_\tau = \tfrac{1}{3}\xi H_\xi + \tfrac{1}{2}(H^2 G_\xi)_\xi, \quad \tau G_\tau = [G(\tfrac{1}{3}\xi + HG_\xi)]_\xi. \tag{4.4a, b}$$

Since G_τ appears to be an order of magnitude smaller than H_τ, we suppose that across the upstream boundary layer, at leading order,

$$\tfrac{1}{3}\xi + HG_\xi = 0. \tag{4.5}$$

This may be substituted into (4.4*a*) to give an equation in $H(\xi,\tau)$ alone. The time dependence in this equation can be eliminated by supposing that

$$H(\xi,\tau) = \frac{\hat{H}(\hat{\xi})}{\tau^\mu}, \quad \xi = \frac{\hat{\xi}}{\tau^\mu}. \tag{4.6}$$

It then follows immediately that $\mu = \frac{1}{6}$. The accuracy of this prediction is demonstrated in the inset in the lowest panel of figure 2 (*b*), which shows $\log(H(0,\tau))$ as a function of $\log\tau$; the circles show computed results, the reference line has a slope of $-\frac{1}{6}$. Thus the width of this boundary layer diminishes roughly as $\tau^{-\frac{1}{6}}$ in (ξ,τ)

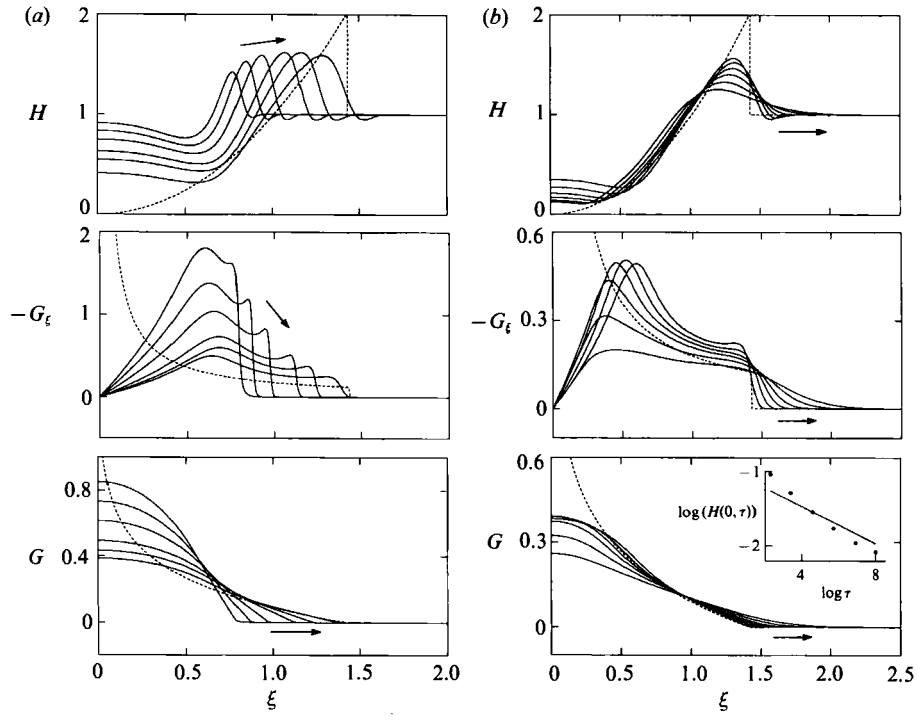

FIGURE 3. The evolution of an axisymmetric drop. The coordinates used are $\xi = x/t^{\frac{1}{6}}$, $H = h$, $G = t^{\frac{1}{3}}\Gamma$ and $G_\xi = t^{\frac{2}{3}}\Gamma_x$. (*a*) and (*b*) show solutions at the same times and for the same parameter values as in figure 2. $\cdots$, the corresponding similarity solution. The slope of the line in the inset in the lowest panel of (*b*) is $-\frac{1}{8}$.

coordinates (and of course grows as $t^{\frac{1}{6}}$ in (x, t) coordinates). The film thins behind the shock also as $t^{-\frac{1}{6}}$, and so will not reach zero in finite time.

4.2 *Axisymmetric drop*

Figure 3(*a*, *b*) shows the evolution of a spreading axisymmetric drop of surfactant. The initial conditions, parameter values and times are exactly as above. Many features of the drop's behaviour resemble the spreading strip. There is an initial transient phase as the solution evolves from the initial condition towards the similarity state (figure 3*a*). A decaying boundary layer at the upstream end of the monolayer persists thereafter (figure 3*b*); an argument similar to that used above predicts that the boundary layer narrows, and the film thins, at a rate of $\tau^{-\frac{1}{8}}$. The insert in the lowest panel of figure 3(*b*) shows that in this case, however, the approximation is less accurate, which is reflected by the fact that G_τ is not as small as for the strip. At early times there exist waves due to capillarity in the film height ahead of the shock, and a weak peak in surface shear stress just behind the stock. These disappear slightly more rapidly than in the strip computation.

Apart from the obvious difference in the shape of the similarity solution, the significant difference with the previous case is that the rate at which the diffusive lengthscale grows is much greater. The maximum film height is never as great as before (this is due to some extent to differences in the shapes of the similarity solutions), and it falls more quickly. It can be seen to fall even in figure 3(*a*), before the similarity state has been attained. For times greater than about 1000 (figure 3*b*) the similarity solution is a poor approximation to the numerical solution, and the

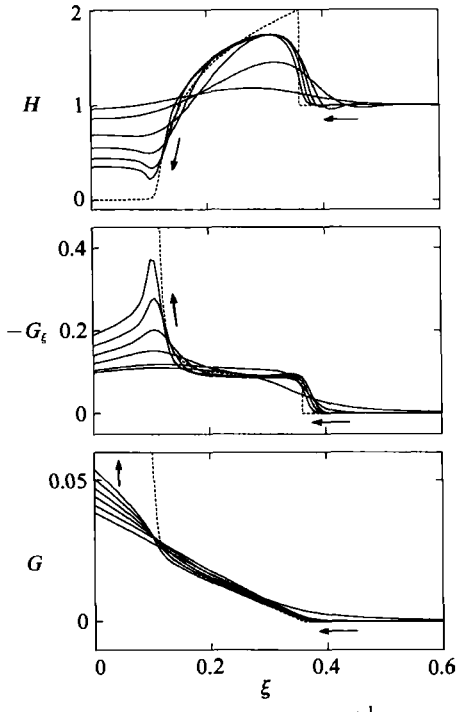

FIGURE 4. The evolution of a planar front. Here $\xi = x/t^{\frac{1}{2}}$, $H = h$, $G = \Gamma$ and $G_\xi = \Gamma_x t^{\frac{1}{2}}$, $\cdots$, the corresponding similarity solution. The times shown are 3, 10, 100, 10^3, 10^4 and 10^5. Parameter values are as in figure 2 except that $\mathscr{D} = 10^{-3}$.

effect of diffusion appears to be confined no longer to a thin region at the shock. Its influence is apparent, for example, in the distribution of surfactant near $\xi = 0$: in its absence, $G(0,\tau)$ remains almost constant and $-G_\xi(0,\tau)$ increases ($10 < \tau < 100$, figure 3*b*); at later times it causes $G(0,\tau)$ and $-G_\xi(0,\tau)$ to fall rapidly.

4.3 *Planar front*

The evolution of the solution is rather different in this case (see figure 4) to the two preceding examples (the only difference in parameter values to the preceding cases is that $\mathscr{D} = 0.001$; in this case $\xi_w = 0.25$). Surfactant is supplied at a rate of $t^{\frac{1}{2}}$ at $\xi = 0$, and from (4.1) there is therefore a surface shear stress at $\xi = 0$ that drives a flow from $\xi < 0$. The film therefore wells up to form a shock much more rapidly than it thins. As time progresses, however, thinning occurs over the upstream 30% of the monolayer. The width of this thinning region no longer decreases like some power of τ, but is instead constrained by the shape of the similarity solution. The upstream boundary condition requires the surfactant concentration to rise slowly at $\xi = 0$, while the flux of surfactant at the origin decreases with time (recall that $-\Gamma_x = -G_\xi/t^{\frac{1}{2}}$).

As the monolayer advances, the gradient of surfactant concentration appears to steepen near its leading edge to form a shock. (The steepening is an artifact of the similarity scaling; surfactant gradients are always diminishing because the front is advancing.) A similarity solution is shown for comparison as a dotted line. As before, capillary forces give rise to a weak wavetrain in H ahead of the shock, that narrows and decays very rapidly; there is very little evidence of a peak in $-G_\xi$ behind the shock. Whereas in both previous examples diffusion ultimately caused a broadening

of the shock and a reduction in the maximum film height, in this case no such behaviour is observed. The solution instead evolves to a state in which the shape of H and $-G_\xi$ at the shock vary very little over long timescales.

5. Asymptotic structure of the shock

The numerical solutions have revealed a number of significant features of the shock structure: at early times a capillary wavetrain exists ahead of it, and a corresponding peak in the shear stress lies behind it; these features disappear as time progresses and the shock speed diminishes; for the strip and the drop, the shock is gradually destroyed by growing diffusive forces, whereas the shock appears to persist indefinitely in the frontal-spreading case. In this section we will use asymptotic methods to explain and quantify these observations, and to establish the timescales over which the similarity solutions provide reasonable approximations to the full problem.

In addition to diffusive and capillary effects, described respectively in §§5.2 and 5.3, we take account also of the effects of a vertical gravitational field, which can play a significant role in the long-term development of the solution (§5.4). Additional effects are considered in the Appendices: in Appendix A it is shown how the presence of a very weak concentration of surfactant on the film ahead of the monolayer smooths the shock, and how it can ultimately halt the advance of the monolayer; the importance of additional effects such as surface viscosity and inertia, usually negligible in the lubrication-theory approximation but here singular perturbations, are considered in Appendix B, and shown to be potentially significant at early times.

5.1. *Scalings at the shock*

In order to understand how the shock at the leading edge of an advancing surfactant monolayer is affected by weak diffusive, capillary and gravitational forces, we move to a frame in which the shock is stationary, and reformulate the governing equations in an inner coordinate system having an arbitrary lengthscale $X(t)$. Let us write

$$x = x_s(t) + X\hat{\xi}, \quad t = T, \quad h(x,t) = H(\hat{\xi}, T), \quad \Gamma(x,t) = \frac{X}{t^{a+b}} G(\hat{\xi}, T), \tag{5.1}$$

where $x_s(t) = \xi_s t^a$ is the position of the shock (recall from §3 that $2a+b=1$). Note that in this inner region the surfactant concentration is scaled so that with $G_{\hat{\xi}} = O(1)$, it will match with the outer similarity solution (scaled by 3.5). We shall require of course that $\mathscr{G} \ll 1, \mathscr{S} \ll 1, \mathscr{D} \ll 1$, and that $X(t) \ll x_s(t)$. Using (5.1), the governing equations (2.15) (with $\mathscr{A} = 0$ and $\mathrm{d}\sigma/\mathrm{d}\Gamma = -1$) become

$$(X H_T - \hat{\zeta} H_{\hat{\zeta}} \dot{X})\, T^{a+b} = a\xi_s H_{\hat{\zeta}} + \tfrac{1}{2}(H^2 G_{\hat{\zeta}})_{\hat{\zeta}} + \left(\frac{\mathscr{G} T^{a+b}}{3X}\right)(H^3 H_{\hat{\zeta}})_{\hat{\zeta}} - \left(\frac{\mathscr{S} T^{a+b}}{3X^3}\right)(H^3 H_{\hat{\zeta}\hat{\zeta}\hat{\zeta}})_{\hat{\zeta}}, \tag{5.2a}$$

$$(X G_T - \hat{\zeta} G_{\hat{\zeta}} \dot{X}) T^{a+b} + \left(\frac{X}{T^{a+b}}\right)_T T^{2(a+b)} G = a\xi_s G_{\hat{\zeta}} + (HGG_{\hat{\zeta}})_{\hat{\zeta}} + \left(\frac{\mathscr{G} T^{a+b}}{2X}\right)(GH^2 H_{\hat{\zeta}})_{\hat{\zeta}} - \left(\frac{\mathscr{S} T^{a+b}}{2X^3}\right)(GH^2 H_{\hat{\zeta}\hat{\zeta}\hat{\zeta}})_{\hat{\zeta}} + \left(\frac{\mathscr{D} T^{a+b}}{X}\right) G_{\hat{\zeta}\hat{\zeta}}. \tag{5.2b}$$

Equation (5.2) is exact for a planar geometry, and a leading-order approximation in an axisymmetric geometry. This is because the lengthscale of the inner region is

always much smaller than the length of the monolayer ($X \ll x_s$), so the curvature of the shock has a negligible influence on the structure of the inner layer.

From (5.2) it is clear that the lengthscales over which gravitational, capillary and diffusive forces balance viscous and Marangoni forces are given respectively by

$$X_{\mathscr{G}} = \mathscr{G}T^{a+b}, \quad X_{\mathscr{S}} = (\mathscr{S}T^{a+b})^{\frac{1}{3}}, \quad X_{\mathscr{D}} = \mathscr{D}T^{a+b}. \tag{5.3}$$

We define the following times at which the various lengthscales of the problem are of the same order:

$$\begin{aligned} T_{\mathscr{D}} &= \mathscr{D}^{-1/b} \quad \text{at which} \quad X_{\mathscr{D}} \sim x_s; \\ T_{\mathscr{D}\mathscr{S}} &= \left(\frac{\mathscr{S}}{\mathscr{D}^3}\right)^{1/(1+b)} \quad \text{at which} \quad X_{\mathscr{D}} \sim X_{\mathscr{S}}. \end{aligned} \tag{5.4}$$

$T_{\mathscr{G}}$ and $T_{\mathscr{G}\mathscr{S}}$ are defined similarly, with $\mathscr{D}$ replaced by $\mathscr{G}$ in (5.4). For times of order 1 or greater, $X_{\mathscr{S}}$ is always much smaller than x_s. Note that $T_{\mathscr{D}\mathscr{S}} \ll T_{\mathscr{D}}$, and that

$$\left.\begin{aligned} X_{\mathscr{D}} \ll X_{\mathscr{S}} \ll x_s \quad &\text{for} \quad T \ll T_{\mathscr{D}\mathscr{S}}, \\ X_{\mathscr{S}} \ll X_{\mathscr{D}} \ll x_s \quad &\text{for} \quad T_{\mathscr{D}\mathscr{S}} \ll T \ll T_{\mathscr{D}}, \\ X_{\mathscr{S}} \ll x_s \ll X_{\mathscr{D}} \quad &\text{for} \quad T_{\mathscr{D}} \ll T. \end{aligned}\right\} \tag{5.5}$$

Again, similar relations hold in (5.5) with $\mathscr{D}$ replaced by $\mathscr{G}$.

Before proceeding further, we must estimate the size of the terms on the left-hand side of (5.2). With $X = X_{\mathscr{D}}$, for example, the terms $\dot{X}T^{a+b}$ are proportional to $\mathscr{D}T^b$. The requirement that $X_{\mathscr{D}} \ll x_s$, i.e. that $\mathscr{D}T^b \ll 1$, ensures that these terms are negligible. The term $(X/T^{a+b})_T$ vanishes identically when $X = X_{\mathscr{D}}$. Similar arguments show that these terms are small when $X = X_{\mathscr{G}}$ or $X = X_{\mathscr{S}}$. We must assume that the remaining terms involving H_T and G_T are also small: this assumption is supported by numerical results, which have shown the similarity solution to be attracting. We can then proceed with a quasi-steady approximation, regarding T merely as a parameter and ignoring effects due to changes in lengthscales at the shock, i.e. with the left-hand side of (5.2) set to zero.

At this stage it is convenient to rescale (5.2) to remove explicit dependence on the outer solution (the factor $a\xi_s$), which is done by setting $\zeta = \hat{\zeta}a\xi_s$ and $\hat{X}_{\mathscr{S}} = X_{\mathscr{S}}(a\xi_s)^{\frac{2}{3}}$. The boundary conditions appropriate to the rescaled equations describing the structure of the inner solution at the shock are then

$$H \to 1, \quad G \to 0 \qquad \text{as} \quad \zeta \to \infty \tag{5.6a}$$

$$H \to 2, \quad G \sim -\tfrac{1}{2}\zeta \quad \text{as} \quad \zeta \to -\infty. \tag{5.6b}$$

With the terms on its left-hand side neglected, (5.2) may be integrated once which, using (5.6), gives

$$H + \tfrac{1}{2}H^2G_\zeta + \tfrac{1}{3}\left(\frac{X_{\mathscr{G}}}{X}\right)H^3H_\zeta - \tfrac{1}{3}\left(\frac{\hat{X}_{\mathscr{S}}}{X}\right)^3 H^3H_{\zeta\zeta\zeta} = 1, \tag{5.7a}$$

$$G + HGG_\zeta + \tfrac{1}{2}\left(\frac{X_{\mathscr{G}}}{X}\right)GH^2H_\zeta - \tfrac{1}{2}\left(\frac{\hat{X}_{\mathscr{S}}}{X}\right)^3 GH^2H_{\zeta\zeta\zeta} + \left(\frac{X_{\mathscr{D}}}{X}\right)G_\zeta = 0. \tag{5.7b}$$

It is worth noting that (5.7b) is at first sight not consistent with (5.6b): the final diffusive term in (5.7b) does not vanish as $\zeta \to -\infty$, leaving an $O(1)$ imbalance. This turns out not to be a difficulty, however, as solutions of (5.7) always satisfy (5.6b) at leading order, i.e. at $O(\zeta)$ in G.

We now examine how the structure of the shock depends on the relative sizes of the governing parameters, and determine the timescales over which different forces

balance. It is clear first of all that if $b > 0$, as it is for a strip or a drop (see 3.4), then $T_{\mathscr{G}}$ and $T_{\mathscr{D}}$ are finite (5.4), because $X_{\mathscr{D}}$ and $X_{\mathscr{G}}$ grow faster than x_s. This means that the shock will be destroyed in finite time by either diffusive or gravitational forces. Thus we expect that with $\mathscr{D} = 0.002$ and $\mathscr{G} = 0$ (as in the computations in §4.1 and §4.2), diffusion will destroy the shock at the leading edge of a strip (drop) in a time $T_{\mathscr{D}} \sim O(10^8)\,(O(10^5))$; these times are consistent with the numerical results in figures 2(*b*) and 3(*b*). For a planar front, however, $b = 0$ so that the diffusive and gravitational lengthscales grow at the same rate as the length of the monolayer, explaining why the shock in figure 4 persists indefinitely with negligible change in structure.

At sufficiently small times the capillary lengthscale $\hat{X}_{\mathscr{S}}$ will always exceed both $X_{\mathscr{D}}$ and $X_{\mathscr{G}}$. For times much in excess of $T_{\mathscr{D}\mathscr{S}}$ or $T_{\mathscr{G}\mathscr{S}}$, however, capillary effects will be swamped by diffusion or gravity. This, also, corresponds with the numerical results of §4. The disappearance of the capillary wavetrain ahead of the shock occurs roughly at $T_{\mathscr{D}\mathscr{S}}$ in each case: for the strip, $T_{\mathscr{D}\mathscr{S}} \approx 1000$ (figure 2*b*); for the drop $T_{\mathscr{D}\mathscr{S}} \approx 500$ (figure 3*b*); for the front $T_{\mathscr{D}\mathscr{S}} \approx 10^5$ (figure 4).

We postpone discussion of the effects of gravity to §5.4. The next two subsections concern the interaction of diffusive and capillary forces, so that we assume that $\mathscr{G} \ll \mathscr{D}$. We begin in §5.2 by examining the situation in which $X_{\mathscr{D}} \gg \hat{X}_{\mathscr{S}}$, i.e. for $T_{\mathscr{D}\mathscr{S}} \ll T \ll T_{\mathscr{D}}$; in this case the surfactant distribution is smoothed by diffusion, and because diffusive, viscous and Marangoni forces are of the same order the film height is smoothed also; capillary effects are negligible. At earlier times, however (i.e. $T \ll T_{\mathscr{D}\mathscr{S}}$), $\hat{X}_{\mathscr{S}} \gg X_{\mathscr{D}}$ so that capillary forces are responsible for smoothing the film height. Although the surfactant distribution is affected by these forces, a discontinuity in its gradient remains which is smooth by diffusion over the much smaller lengthscale $X_{\mathscr{D}}$. This situation is described in §5.3. The monolayer's behaviour at late times, when $T \gg T_{\mathscr{D}}$ and $X_{\mathscr{D}} \gg x_s$, will be considered in §6 below.

5.2 *Purely diffusive inner layer*

Setting $X = X_{\mathscr{D}}$ in (5.7) with $X_{\mathscr{G}} \ll X_{\mathscr{D}}$ and $\hat{X}_{\mathscr{S}} \ll X_{\mathscr{D}}$ gives, at leading order,

$$H + \tfrac{1}{2}H^2 G_\zeta = 1, \quad G + HGG_\zeta + G_\zeta = 0. \tag{5.8}$$

Choosing the signs of square roots to be consistent with the boundary conditions (5.6), (5.8) may be rearranged so that

$$H = 1 - \frac{1}{G} + \left(1 + \frac{1}{G^2}\right)^{\frac{1}{2}}, \quad G_\zeta = G^2 - (G^2 + G^4)^{\frac{1}{2}}. \tag{5.9a, b}$$

(5.9*b*) may integrated to give

$$\sinh^{-1}\left(\frac{1}{G}\right) - \coth\left(\tfrac{1}{2}\sinh^{-1}\left(\frac{1}{G}\right)\right) = \zeta - \zeta_0, \tag{5.10}$$

where ζ_0 is an constant of integration that may be set to zero without loss of generality. This inner diffusive solution, which corresponds exactly to that obtained by BG, is shown in figure 5. Ahead of the shock, H and G decay exponentially, whereas behind it they decay algebraically, explaining why the shock has a very sharp leading edge and much smoother shape behind. The inner solution in figure 5 clearly captures the large-time shock structure shown in figures 2(*b*) ($t > 1000$) and 4 ($t > 10^4$), for example. (Note that because $X_{\mathscr{D}}$ and x_s grow at the same rate for a spreading front, the effects of diffusion could have been included in the computation of the similarity solution, i.e. in determining the fixed points of (3.7).)

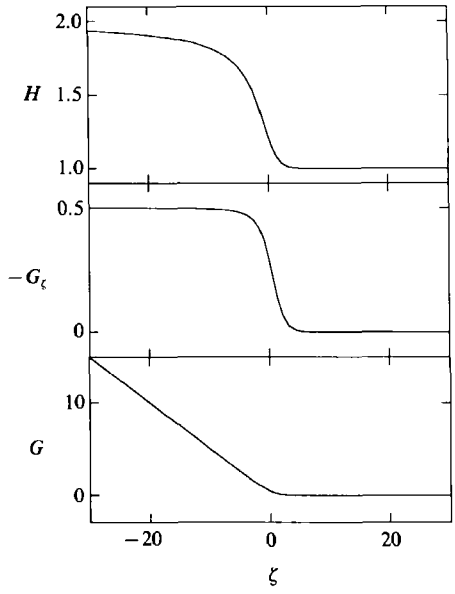

FIGURE 5. The diffusive inner-layer solution satisfying (5.8), showing film height, shear stress and surfactant distribution.

5.3. *Capillary inner layer, diffusive sublayer*

Setting $X = \hat{X}_{\mathscr{S}}$ in (5.7) with $X_{\mathscr{G}} \ll \hat{X}_{\mathscr{S}}$ and $X_{\mathscr{D}} \ll \hat{X}_{\mathscr{S}}$ gives

$$\left.\begin{aligned} H + \tfrac{1}{2}H^2 G_\zeta - \tfrac{1}{3}H^3 H_{\zeta\zeta\zeta} &= 1, \\ G + HGG_\zeta - \tfrac{1}{2}GH^2 H_{\zeta\zeta\zeta} + \delta G_\zeta &= 0, \end{aligned}\right\} \tag{5.11}$$

where $\delta = X_{\mathscr{D}}/\hat{X}_{\mathscr{S}}$. Although $\delta \ll 1$ for $T \ll T_{\mathscr{D}\mathscr{S}}$, diffusive effects are important over a thin, but growing, sublayer of width δ in the scaling of (5.11). Diffusion smooths the discontinuity in shear stress over this narrow region while capillarity smooths the film height over a region of width $(O(1)$.

Neglecting the diffusive term, (5.11) can be rearranged as follows. There are two possible solutions, one in which

$$H_{\zeta\zeta\zeta} = \frac{6(H-2)}{H^3}, \quad G_\zeta = \frac{-2(3-H)}{H^2}, \tag{5.12a}$$

and the other in which

$$H_{\zeta\zeta\zeta} = \frac{3(H-1)}{H^3}, \quad G = 0. \tag{5.12b}$$

(The equation for H in (5.12b) corresponds to one which arises frequently in problems involving capillary forces acting on translating free surfaces of thin viscous films, and is discussed by Bretherton (1961), for example.) The solution of (5.11) is obtained by patching together the appropriate solutions of (5.12a) upstream of $\zeta = 0$, say, and (5.12b) downstream.

Before computing this solution it is useful to determine the asymptotic structure of the solutions of (5.12) in the limits $\zeta \to \pm\infty$. Linearizing H about 2 and about 1 in each case, and choosing solutions consistent with the boundary conditions (5.6), we find that as $\zeta \to -\infty$,

$$H \sim 2 - C_1 \exp[(\tfrac{3}{4})^{\frac{1}{3}}\zeta], \quad G \sim -\tfrac{1}{2}\zeta - \tfrac{1}{2}C_1(\tfrac{4}{3})^{\frac{1}{3}} \exp[(\tfrac{3}{4})^{\frac{1}{3}}\zeta], \tag{5.13}$$

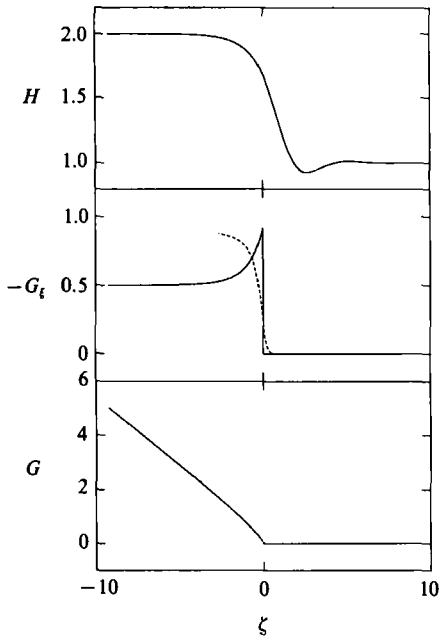

FIGURE 6. ——, The capillary inner-layer solution satisfying (5.12); – – –, a solution of the diffusive sublayer equations (5.15).

and as $\zeta \to \infty$,

$$H \sim 1 + \exp\left(-\frac{3^{\frac{1}{3}}}{2}\zeta\right)[C_2 \cos(\tfrac{1}{2}3^{\frac{5}{3}}\zeta) + C_3 \sin(\tfrac{1}{2}3^{\frac{5}{3}}\zeta)], \quad G = 0, \tag{5.14}$$

where C_1, C_2 and C_3 are arbitrary constants.

This solution has been obtained numerically and is shown with solid lines in figure 6. The procedure used to compute this solution was to take some initial value ζ_0 far upstream of the shock, and to integrate (5.12*a*) downstream using (5.13) as an initial condition, choosing some value of C_1. This integration was stopped as soon as G reached zero (at which point $H = H_c$, say), and then resumed using (5.12*b*). The value of C_1 was varied until a solution of the form (5.14) was obtained for large positive values of ζ. Since ζ_0 was arbitrary, the shock could then be repositioned at $\zeta = 0$.

The solution of (5.11) has discontinuities in $H_{\zeta\zeta\zeta}$ and Γ_ζ that are smoothed over a thin diffusive sublayer of width δ. The structure of the solution in this region is revealed if we take $\zeta = \delta\bar{\zeta}$, $H(\zeta) = H_c + \delta^3\bar{H}(\bar{\zeta})$ and $G(\zeta) = \delta\bar{G}(\bar{\zeta})$. To leading order, this gives

$$H_c + \tfrac{1}{2}H_c^2\bar{G}_{\bar{\zeta}} - \tfrac{1}{3}H_c^3\bar{H}_{\bar{\zeta}\bar{\zeta}\bar{\zeta}} = 1, \tag{5.15a}$$

$$\bar{G} + H_c\bar{G}\bar{G}_{\bar{\zeta}} - \tfrac{1}{2}\bar{G}H_c^2\bar{H}_{\bar{\zeta}\bar{\zeta}\bar{\zeta}} + \bar{G}_{\bar{\zeta}} = 0. \tag{5.15b}$$

(5.15) may be integrated to give $\bar{G}(\bar{\zeta})$:

$$\tfrac{1}{2}\left(\frac{3}{H_c} - 1\right)\bar{\zeta} + \tfrac{1}{4}H_c\bar{G} + \log\bar{G} = 0. \tag{5.16}$$

This inner solution is shown as a dotted line in figure 6; its predominant effect is to smooth G_ζ.

This asymptotic solution contains the important features of a sizable class of solutions of the partial differential equations (figure 2, $2 \leqslant t \leqslant 30$; figure 3, $2 \leqslant t \leqslant 10$; figure 4, $10 \leqslant t \leqslant 100$). Notice that for the strip and the front, the capillary lengthscale decreases in the coordinate systems of figures 2 and 4, but for the drop it is constant (figure 3). Ahead of the shock lies a train of decaying waves with a structure approximately by (5.14). Behind the shock the inner solution decays exponentially, suggesting that the height of the film will be greater than in the purely diffusive case described in §5.2. Within the inner region in which Marangoni and capillary forces are balanced, the portion of the surface covered by surfactant must have surface velocity equal to the shock speed. This balance is implicit in (5.12a), and is responsible for the steepening of the surfactant distribution just behind the shock. The large discontinuity in surface shear stress is smoothed off by diffusion at the shock. Ahead of the shock, where $\Gamma = 0$, the direction of the velocity field is determined entirely by the sign of $H_{\zeta\zeta\zeta}$, and from (5.12b) this implies that the flow is forward for $H > 1$ and reversed for $H < 1$.

5.4. *The effects of gravity*

Gravity plays a minor role in the evolution of the shock when $\mathscr{G} \approx \mathscr{D}$. At small times ($T \ll T_{\mathscr{D}\mathscr{S}}$) there is a wide capillary inner layer and smaller sublayer in which diffusive and gravitational forces are apparently of the same size. However, while diffusion remains a singular perturbation (smoothing the discontinuity in shear stress), the film is smoothed by capillarity, so that gravity provides only a weak, regular perturbation to the solution described in §5.3. Gravity is more important at larger times ($T_{\mathscr{D}\mathscr{S}} \ll T \ll T_{\mathscr{D}}$), when it balances diffusion in an inner layer; capillarity is no longer significant in this case. Solutions for this inner layer, parameterized by $\bar{\delta} = \mathscr{D}/\mathscr{G}$, may be determined straightforwardly, but it is only once $\bar{\delta}$ becomes small (with $\mathscr{G} \gg \mathscr{D}$) that significant differences to the purely diffusive case (figure 5) are evident, so we restrict our attention to this case.

Let us therefore suppose that $\bar{\delta} \ll 1$ and that $T_{\mathscr{D}\mathscr{S}} \ll T \ll T_{\mathscr{G}}$, so that $\hat{X}_{\mathscr{S}} \ll X_{\mathscr{D}} \ll X_{\mathscr{G}} \ll x_s$, making capillary effects negligible. Setting $X = X_{\mathscr{G}}$ in (5.7) we obtain

$$\left.\begin{aligned} H + \tfrac{1}{2}H^2 G_\zeta + \tfrac{1}{3}H^3 H_\zeta &= 1, \\ G + (GH + \bar{\delta})G_\zeta + \tfrac{1}{2}GH^2 H_\zeta &= 0. \end{aligned}\right\} \tag{5.17}$$

Although $\bar{\delta}$ is small, it multiplies a singular term, and the situation is similar to that in §5.3: the film height is smoothed across a gravitational inner layer, and the surfactant distribution is smoothed across a narrower diffusive sublayer.

Setting $\bar{\delta} = 0$ in (5.17) gives two sets of equations, with solutions which may be patched together across $\zeta = 0$, say. Upstream of this point,

$$H_\zeta = \frac{6(2-H)}{H^3}, \quad G_\zeta = -\frac{2(3-H)}{H^2}, \tag{5.18a}$$

while downstream

$$H_\zeta = \frac{3(1-H)}{H^3}, \quad G = 0. \tag{5.18b}$$

Since $H \to 2$ as $\zeta \to -\infty$, we must have $H = 2$, $G = -\frac{1}{2}\zeta$ for $\zeta < 0$, as $H = 2$ is a stable fixed point of (5.18a). Across $\zeta = 0$, H and G are continuous but their first derivatives are not. In $\zeta > 0$ H decreases monotonically from 2 to 1, according to

$$H + \tfrac{1}{2}H^2 + \tfrac{1}{3}H^3 + \log(H-1) = \tfrac{1}{3}(20 - 9\zeta); \tag{5.19}$$

clearly H diminishes exponentially far ahead of the shock.

To smooth the discontinuities in G_ζ and H_ζ at $\zeta = 0$, (5.17) may be rescaled using $\zeta = \bar{\delta}\bar{\zeta}$, $H = 2+\bar{\delta}\bar{H}(\bar{\zeta})$ and $G = \bar{\delta}\bar{G}(\bar{\zeta})$. The equations governing the solution in this innermost diffusive layer reduce at leading order to

$$\bar{H}_{\bar{\zeta}} = \frac{-3}{2(4+2\bar{G})}, \quad \bar{G}_{\bar{\zeta}} = \frac{-\bar{G}}{(4+2\bar{G})}, \tag{5.20}$$

which has a solution equivalent to (5.16) with H_c replaced by 2, thus resembling the dotted curve on figure 6.

At earlier times ($T_{\mathscr{GS}} \ll T \ll T_{\mathscr{DS}}$), $X_{\mathscr{D}} \ll \bar{X}_{\mathscr{S}} \ll X_{\mathscr{G}}$, so that the discontinuity in H_ζ is smoothed over the capillary lengthscale, and the discontinuity in G_ζ is smoothed over the smaller diffusive lengthscale, but the basic features of the solution correspond to the situation described above. Before this ($T \ll T_{\mathscr{GS}}$) capillarity smooths the film and gravity is not significant. Thus, with $\mathscr{D} \ll \mathscr{G}$ we conclude that for $T \ll T_{\mathscr{G}}$ the surfactant distribution at the leading edge of the monolayer is always controlled by diffusion, but that when $T_{\mathscr{GS}} \ll T \ll T_{\mathscr{G}}$ the disturbance to the film extends $O(X_{\mathscr{G}})$ ahead of the leading edge of the monolayer. We have confirmed that this corresponds with numerical solutions of (2.15).

6. Diffusive spreading

If $\mathscr{D} \ll 1$ and $\mathscr{G} \ll 1$, we have seen that the shock at the leading edge of a spreading strip or drop of surfactant is destroyed in finite time by either diffusive or gravitational forces, depending on the relative sizes of $\mathscr{D}$ and $\mathscr{G}$. In this section we consider the situation in which diffusion ultimately becomes the dominant mode of surfactant transport. We consider cases in which either $\mathscr{D} \ll 1$ (when we require $\mathscr{G} \ll \mathscr{D}$) or in which $\mathscr{D} = O(1)$ or larger (and $\mathscr{G} \ll 1$). In either case diffusion requires a finite time to become significant everywhere in the flow, and to be no longer confined to a boundary layer at the leading edge of the monolayer: this is the time at which the coefficient of the diffusive term in (3.7*b*) is no longer small

$$\mathscr{D}t^b \gg 1, \tag{6.1}$$

where b is given by (3.4). It is clear from (5.4) that (6.1) implies that $X_{\mathscr{D}} \gg x_s$. With (6.1) satisfied, diffusion governs the surfactant distribution, and Marangoni forces then determine the corresponding film shape. To express this balance, we write

$$\eta = \frac{x}{(\mathscr{D}t)^{\frac{1}{2}}}, \quad T = t, \tag{6.2}$$

and

$$\Gamma(x,t) = \frac{\mathscr{D}G(\eta,T)}{(\mathscr{D}t^b)^\nu}, \quad h(x,t) = 1+\frac{H(\eta,T)}{(\mathscr{D}t^b)^\nu}, \tag{6.3}$$

where $\nu = \frac{3}{2}$ in a planar geometry and $\nu = 2$ in axisymmetry. This scaling assumes the mass of surfactant (3.1) is given by (3.2). Substituting these expressions into (2.15) (setting $\mathscr{G} = \mathscr{S} = \mathscr{A} = 0$) gives

$$TH_T = b\nu H + \tfrac{1}{2}\eta H_\eta + \tfrac{1}{2}\partial_\eta(G_\eta) + O\left(\frac{1}{(\mathscr{D}t^b)^\nu}\right), \tag{6.4a}$$

$$TG_T = b\nu G + \tfrac{1}{2}\eta G_\eta + \partial_\eta(G_\eta) + O\left(\frac{1}{(\mathscr{D}t^b)^\nu}\right). \tag{6.4b}$$

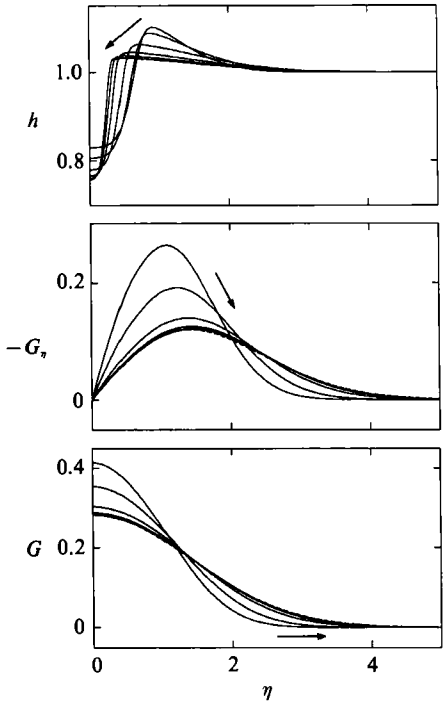

FIGURE 7. The large-time evolution of a planar strip, shown in stretched coordinates $\eta = x/(\mathscr{D}t)^{\frac{1}{2}}$. Film height h, scaled surface shear stress $-G_\eta = -(\mathscr{D}t)\Gamma_x$ and scaled surfactant distribution $G = (\mathscr{D}t)^{\frac{1}{2}}\Gamma$ are shown at times 1.5, 2, 4, 8, 12, 16 (arrows indicate increasing time). The heavy dotted lines in the lower two panels show the corresponding similarity solution (6.5). Parameter values are $\mathscr{D} = 1$, $\mathscr{S} = \mathscr{G} = \mathscr{A} = 0$, $\beta = 100$.

We seek fixed points of (6.4), subject to the boundary conditions $H \to 0, G \to 0$ as $\eta \to \infty$. Simple solutions arise in the case $\alpha = 0$, when it is straightforward to show that

$$H = (Q/c)\exp[-\tfrac{1}{4}\eta^2], \quad G = 2H, \tag{6.5}$$

where $c = 2\pi^{\frac{1}{2}}$ for a spreading strip and $c = 8\pi$ for a spreading drop.

The validity of this asymptotic result (6.5) can be tested against numerical solutions of the full governing equations. Typical solutions, recast in (η, T) coordinates (using 6.2) and with Γ scaled appropriately (using 6.3), are shown in figure 7. $\mathscr{D} = 1$ in this calculation, so that the surfactant distribution evolves rapidly to its predicted form; the computed values of G and G_η are almost indistinguishable from (6.5) (shown as heavy dotted lines in the figure) for $T \geqslant 12$. The film height behaves as expected over the majority of its range. The boundary condition $H_\eta = 0$ at $\eta = 0$, however, is not consistent with (6.5) and so a thinning boundary layer is present across which the upstream boundary condition is accommodated.

7. Film rupture

Although the film deformations induced by a spreading monolayer can be very large, we have demonstrated that when subject to viscous and Marangoni forces alone, the dramatic thinning of the film beneath the monolayer is never sufficient to drive the film to rupture in finite time. Indeed, the numerical results in §4 indicated that the rate at which the film thins beneath a strip (drop) of spreading surfactant

is approximately $t^{-\frac{1}{6}}$ ($t^{-\frac{1}{8}}$); it was also demonstrated that the corresponding length of the depression in film height behind the shocks grew as $t^{\frac{1}{6}}$ ($t^{\frac{1}{8}}$). These predictions were not strongly dependent on the initial distribution of surfactant.

Nevertheless, rupture of the film shortly after surfactant is deposited on its upper surface has been observed in experiments (GG2; Ahmad & Hansen 1972). An additional mechanism must be responsible for these observations. In this section, we examine a likely candidate: van der Waals forces, operating through the terms proportional to $\mathscr{A}$ in (2.15). We hypothesize that rupture arises through a two-part process: first, the thinning of the film due to Marangoni effects is sufficiently vigorous to reduce the minimum film thickness to less than 1000 Å, the thickness beneath which van der Waals forces are effective; second, an instability due to these forces (Ruckenstein & Jain 1974; Williams & Davis 1982) drives the film thickness to zero at some point. The minimum film heights achieved in the numerical simulations of §4 by $O(1)$ times are generally no less than about one tenth of the undisturbed film height, indicating that, with thinning as described by this model, rupture cannot be expected in films of thicknesses greater than about 1 μm. Gravitational forces are not significant in such thin films (since $\mathscr{G}$ is proportional to $\tilde{H}^2$), so we set $\mathscr{G} = 0$ for the remainder of this section. It is important to remember, however, that the film thicknesses used in experiments in which rupture was observed were $O(1$ mm) (GG2; Ahmad & Hansen 1972).

Although Marangoni flows are primarily responsible for the thinning of the film that subsequently results in its disruption, the presence of a surfactant monolayer in fact has a stabilizing effect on a growing rupture instability. The extent to which surfactant inhibits the growth of a deformation of an initially uniform film, in both the linear and nonlinear regimes, is discussed in §7.1. The instability of a spreading monolayer is then examined in §7.2.

7.1. *Stability of a uniform film*

We review first the linear stability of a uniform flight of height h_0 and uniform surfactant concentration Γ_0 (Ruckenstein & Jain 1974; Sharma & Ruckenstein 1986). Let $\alpha = -(\mathrm{d}\sigma/\mathrm{d}\Gamma)\ (\Gamma_0)$, so that $\alpha > 0$. We suppose that $h = h_0 + h_1 \mathrm{e}^{\mathrm{i}kx+st}$, $\Gamma = \Gamma_0 + \Gamma_1 \mathrm{e}^{\mathrm{i}kx+st}$, where $h_1 \ll 1, \Gamma_1 \ll 1$. Substituting these expressions into (2.15) and linearizing, a dispersion relation relating s to k is obtained. Neglecting Marangoni effects (i.e. setting $\alpha = 0$), the competition between van der Waals and capillary forces is expressed by

$$s = (A h_0^{-1})\, k^2 - (\tfrac{1}{3}\mathscr{S} h_0^3)\, k^4. \tag{7.1}$$

All sufficiently long waves are unstable, i.e. $s > 0$ provided $0 < k < k_c = (3\mathscr{A}/\mathscr{S} h_0^4)^{\frac{1}{2}}$; shorter waves are stabilized by capillarity. The effect of insoluble surfactant on the film may be included by considering non-zero α. In this case the dispersion relation becomes rather unwieldy, but one may show that the range of unstable wavenumbers remains unchanged, while the growth rate of instabilities is reduced. The presence of surfactant reduces the wavenumber of the most unstable mode which is reduced by up to 10%. In the limit $\alpha \to \infty$, it may be shown that the growth rate is reduced to exactly $\frac{1}{4}$ of its value when $\alpha = 0$ (given by (7.1)).

The mechanism by which surfactant stabilizes the rupture process is as follows. Consider an initial disturbance to a film on which there is a uniform distribution of surfactant. The potential ϕ (representing intermolecular forces) rises beneath depressions and falls where the film is elevated (see (2.5), (2.7)), so that flows are generated in the film away from depressions towards elevations, causing the original

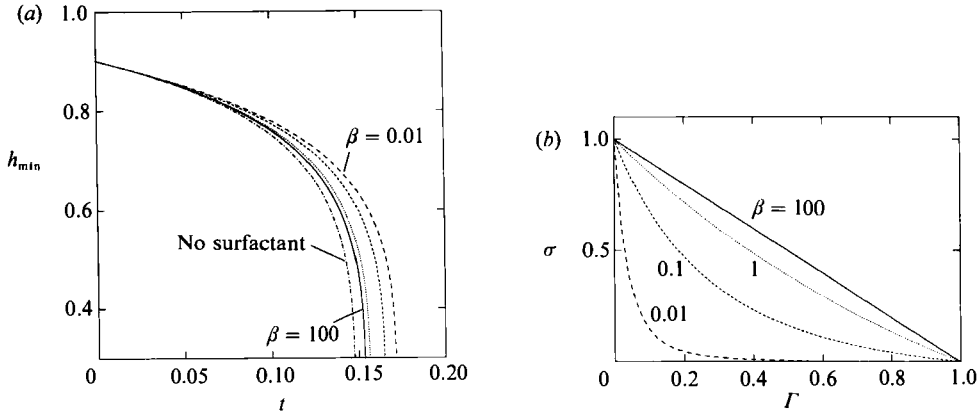

FIGURE 8. The nonlinear evolution of a rupture instability of an initially uniform film is represented in (*a*) by the dependence of minimum film thickness with time. A uniform distribution of surfactant $\Gamma_0 = 0.1$ was present on the surface at $t = 0$. The solutions for values of surfactant activity ---, $\beta = 0.01$; ---, 0.1; · · ·, 1; ——, 100 are compared with —·—, the evolution in the absence of surfactant. Parameter values are $\mathscr{A} = 1$, $\mathscr{S} = 0.1$; 301 grid points covered a domain of length 1, corresponding to a half wavelength of the instability. (*b*) shows how the equation of state (2.2), (2.3), depends on β.

disturbance to grow in amplitude. These flows advect surfactant away from depressions, increasing the surface tension at depressions and decreasing it where the film is elevated, producing gradients of surface tension and hence shear stresses that oppose the flows. Thus surfactant decreases the growth rate of the instability, but does not affect critical wavelengths.

Even once the instability grows in amplitude, the stabilizing influence of surfactant remains relatively weak. This we established by examining numerically the evolution of an initially sinusoidal disturbance of a uniform film, for a range of different equations of state. The parameter values used were $\mathscr{A} = 1$, $\mathscr{S} = 0.1$, $h_0 = 1$, $\Gamma_0 = 0.1$ and the wavelength of the instability was $\lambda = 2\pi/k = 2$, close to the most unstable wavelength for these parameter values ($\lambda = 1.62$ is the most unstable wavelength when $\alpha = 0, \lambda = 1.81$ the most unstable wavelength for $\alpha > 0.$). A nonlinear equation of state ((2.2), (2.3)) was employed, and values of β ranging from 0.01 to 100 were considered. The shape of the different equations of state is shown in figure 8 (*b*). At $t = 0$ the film was given a sinusoidal disturbance of amplitude 0.1. The computations were run until $h_{\min}$ reached 0.3; this was adequate for a reasonable assessment of the time required for the film to rupture. $h_{\min}$ is plotted as a function of time in figure 8 (*a*); it is clear that despite large variations in β, corresponding to a three-fold variation in $\mathrm{d}\sigma/\mathrm{d}\Gamma(\Gamma = \Gamma_0)$, that rupture times were fairly insensitive to the activity of the surfactant, varying by less than 20%.

The presence of a surfactant monolayer will never prevent an instability from developing, and its ability to slow the time taken for a film to rupture appears not to be particularly powerful, in either the linear or the nonlinear regimes.

7.2. *Instability of a spreading monolayer*

Obviously the predictions of linear theory cannot be applied directly to the non-uniform, unsteady film profiles and surfactant distributions of a spreading surfactant monolayer. However, it provides a useful guide to those circumstances in which rupture can be expected to occur. A simple first approximation is to suppose that the

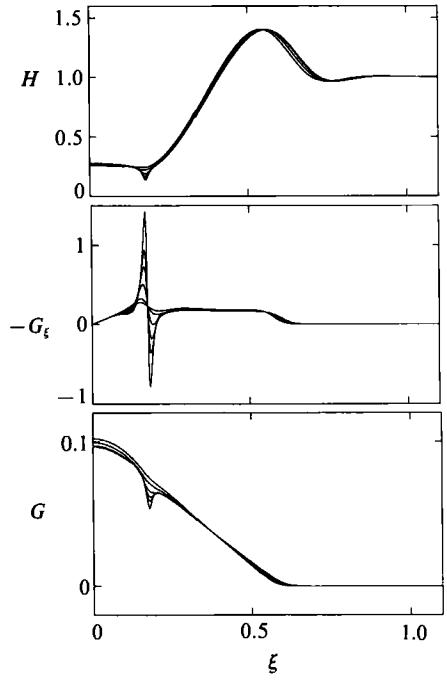

FIGURE 9. The rupture instability of a spreading droplet, shown at times 2.2, 2.4, 2.6, 2.66, 2.68 and 2.695 using the same scaled coordinates and variables as figure 3. Parameter values are $\mathscr{S} = 10^{-4}$, $\mathscr{A} = 10^{-3}$, $\mathscr{D} = 0.002$, $\mathscr{G} = 0$, $\beta = 100$, $G_a = 1$, $\xi_0 = 0.1$, $\xi_w = 0.05$, $N = 301$.

instability grows much faster than the rate at which the film changes its shape. The wavelength of the initial disturbance is roughly proportional to the width of the thinned region; this width must exceed $\lambda_c = 2\pi/k_c \propto (\mathscr{S}h_0^4/\mathscr{A})^{\frac{1}{2}}$ for rupture to be expected. Assuming that $\lambda_m \sim t^{1/\nu}$, and that the minimum film thickness is $O(t^{-1/\nu})$, then rupture can be expected at times at which $\lambda_m \sim \lambda_c$, i.e. at times $t_r \sim (\mathscr{S}/\mathscr{A})^{\nu/6}$. With $\nu = 6$ for a strip, and $\nu = 8$ for a drop, rupture can be anticipated at $O(1)$ times provided $\mathscr{S}$ and $\mathscr{A}$ are of approximately the same order.

This is indeed what is observed numerically. The evolution of a spreading drop in the presence of weak van der Waals forces was determined by computing solutions of (3.7), using exactly the same parameter values as in figure 3 (so that $\mathscr{S} = 10^{-4}$) with the exception of the following: the steepest possible initial conditions were employed, to encourage rapid thinning ($G_\alpha = 1$, $\xi_0 = 0.1$, and $\xi_w = 0.05$ or 0.01 in (4.2)); and $\mathscr{A}$ was set to 10^{-5}, 10^{-4} and 10^{-3}. Using $\xi_w = 0.05$, the computed rupture times corresponding to these values of $\mathscr{A}$ were respectively approximately 180, 16, and 2.7 (integration began at $\tau = 1$). Making the initial surfactant distribution steeper reduced rupture times slightly: with $\xi_w = 0.01$, they became 62, 6.5 and 1.6. Since the evolution of the entire monolayer had to be computed, computational resources were inadequate to carry the calculation to the very final stages of rupture, but were sufficient for a reasonable estimate of rupture time to be made.

Results for the case with $\mathscr{A} = 10^{-3}$ and $\xi_w = 0.05$ are presented in figure 9, at times 2.2, 2.4, 2.6, 2.66, 2.68 and 2.695. Note that similarity variables were used, so that over these times the majority of the solution evolves very little. At the point at which the film is thinnest, however, a rupture instability begins to grow, and a narrow depression in film height develops rapidly. As described above, the pressure gradients

arising from non-uniform intermolecular forces advect surfactant away from the depressed region, and large surface shear stresses develop that oppose the growing instability. The computation was halted once these gradients could no longer be resolved adequately; conservation of mass of surfactant on the upper surface of the film was the condition used to ensure the accuracy of the results.

Comparison of figures 2 and 3 demonstrate the greater propensity of the film beneath a spreading drop to thin compared to that beneath a strip. The time taken for a strip to rupture is correspondingly somewhat greater. With $\xi_w = 0.05$, and setting $\mathscr{A} = 10^{-4}$ (10^{-3}), with all the remaining parameters as in figure 9, the rupture time of a strip was found to be approximately 87 (7.5); all the main features of the flow resembled figure 9.

8. Discussion

The similarity arguments and asymptotic methods of §§3, 5 and 6 have been demonstrated to provide valuable approximations of a substantial class of solutions of the nonlinear evolution equations (2.15). We have shown that if diffusive, gravitational and capillary forces are weak, the rate at which a monolayer of insoluble surfactant spreads is determined, at least initially, by a balance of viscous and Marangoni forces. An axisymmetric drop advances as $t^{\frac{1}{4}}$, a planar strip as $t^{\frac{1}{3}}$ and a planar front (for which surfactant is supplied at a rate of $t^{\frac{1}{2}}$) as $t^{\frac{1}{2}}$ (§3). These rates were predicted also by Espinosa (1991); the drop rate corresponds with a numerical prediction in GG1, and the front rate with the estimate of BG. A shock exists at the leading edge of the monolayer, across which is an abrupt transition in the height of the film, and a corresponding discontinuity in shear stress. As the surfactant spreads, its rate of advance falls, and different balances of forces control the structure of the shock. Initially, capillarity smooths the film; at later stages, either diffusion or gravity determine the form of the shock (§5). For a drop or a strip, at sufficiently large times the effect of these forces is no longer confined to a narrow region, and one or the other eventually dominates the entire spreading process. If diffusion is the more significant, for example, the spreading rate of a drop (strip) changes after a time $O(\mathscr{D}^{-2})$ ($O(\mathscr{D}^{-3})$) to $(\mathscr{D}t)^{\frac{1}{2}}$ (§6). (This prediction is valid for arbitrary $\mathscr{D}$, and corresponds to a numerical result in GG1.) A planar front, on the other hand, will advance subject to the viscous–Marangoni balance indefinitely, provided $\mathscr{D} \ll 1$.

At the upstream end of the monolayer the film becomes progressively thinner, to compensate for the increasing size of the region in which the film is elevated above its undisturbed height. The rate of thinning was estimated in §4, for a film subject to viscous and Marangoni forces alone; it was demonstrated that under these conditions, an infinite time would be required for the film height to fall to zero. Once the film is sufficiently thin, however, intermolecular forces can become significant. It was demonstrated in §7 that, after severe thinning due to Marangoni effects, an instability due to van der Waals forces can cause the film to rupture, provided, however, that these forces were at least of the magnitude of the stabilizing capillary forces (i.e. $\mathscr{S} = O(\mathscr{A})$).

Despite the presence of a shock, in apparent violation of the assumptions of lubrication theory, the model of §2 may be demonstrated *a posteriori* to be consistent at all but the earliest times, not just in the majority of the flow but also in the vicinity of the shock. A variety of terms originally neglected from the model are examined in Appendix B (representing film stretching, inertia and surface viscosity) and are shown to be significant only in the initial stages of spreading. Their effects are always

ultimately suppressed either by capillarity, diffusion or gravity. Clearly the model's predictions at early times, when surface tension gradients are largest, must be interpreted with care.

An additional question of consistency concerns the use of small values of $\mathscr{S}$, despite the requirement that $\mathscr{S} = O(1)$ for the surface tension (2.1) in the normal stress condition (2.10) to be independent of Γ. We found that when $\mathscr{S}$ is small, capillary effects are significant only in the vicinity of the shock, where Γ is very close to 0, so that $\sigma(\Gamma)$ (in (2.1)) is close to 1. The value of the surface tension at the shock is therefore underestimated in (2.10) by an $O(\epsilon^2)$ amount. This inaccuracy has no qualitative significance, however, so it is reasonable to neglect the effects of surfactant on the mean surface tension of the film†.

To test the accuracy and applicability of these results, it is instructive to establish parameter values typical of conditions in experiment and in the lung. Because large variations in physical quantities can be anticipated, particularly in physiological fluids, we make only rough order-of-magnitude estimates. Let us suppose that $\tilde{D} \approx 10^{-5}$ cm^2/s (GG2), $g \approx 10^3$ cm s^{-2}, $\rho \approx 1$ g/cm^3, $\tilde{S} \approx 10$ dyn/cm, $\sigma_m \approx 10$ dyn/cm, $\tilde{A} \approx 10^{-13}$ erg and $\epsilon \approx 10^{-2}$. Film thicknesses and viscosities typical (*a*) of experiment are $\tilde{H} \approx 1$ mm, $\mu \approx 10^{-1}$ g/(cm s) (GG2), (*b*) of airway mucus are $\tilde{H} \approx 10$ μm, $\mu \approx 10^{-1}$ g/(cm s) and (*c*) of alveolar liquid lining are $\tilde{H} \approx 1$ μm, $\mu \approx 10^{-2}$ g/(cm s). In each case $\mathscr{S} = O(10^{-4})$, and the values of $\mathscr{D}$, $\mathscr{G}$, $\mathscr{A}$, and $\epsilon^2 Re$ (see §2) are then respectively: (*a*) $O(10^{-6}, 1, 10^{-12}, 10^{-2})$; (*b*) $O(10^{-4}, 10^{-4}, 10^{-8}, 10^{-4})$; (*c*) $O(10^{-4}, 10^{-6}, 10^{-6}, 10^{-3})$.

Because $\mathscr{G}$ is $O(1)$ in experiments (GG2; Ahmad & Hansen 1972), it controls the spreading rate of a monolayer from the early stages, preventing comparison with the similarity estimates of §3. This accounts for the considerable discrepancy between the predicted spreading rate of a drop of surfactant, $t^{\frac{1}{4}}$ when $\mathscr{G} \ll 1$, and the spreading rates measured by GG2 (they found exponents greater than 0.6). GG2 showed, however, that, using the appropriate value of $\mathscr{G}$, the model of §2 described the experimental results satisfactorily.

What is most surprising about the experimental parameter values is that $\mathscr{A}$ is many orders of magnitude smaller than $\mathscr{S}$. On the basis of the predictions of §7, we would therefore anticipate that film rupture would be an extremely rare event; not only would the relatively large surface tension always stabilize a rupture instability, but the very large gravitational force would always prevent any disturbance from growing. Nevertheless, this is not the case, as rupture was commonly observed by GG2. Its occurrence was strongly related to the initial conditions used in the experiments, however: if a droplet of surfactant was deposited manually on the undisturbed film, rupture would occur provided the film was sufficiently thin (e.g. it was observed when $\tilde{H} = 0.4$ mm); if spreading was initiated by lifting a barrier that surrounded a carefully determined quantity of surfactant already on the surface of the film, then rupture could be avoided. It is worth noting that in the former case a very large amount of surfactant (a 30 μl droplet) was used, only a small portion of which could be expected to form a monolayer. The failure to predict rupture for these parameter values is probably due to two related factors: the inadequacy of the initial condition used in the numerical simulations to represent the collision of a bulk droplet and the film; and the inaccuracy of the model in the early stages of spreading. The importance of the unsteady interaction of droplet and film is supported by

†*Note added in proof:* Recent computations (by F. F. Espinosa, R. D. Kamm, personal communication) in which terms describing the dependency of capillary effects on local surfactant concentration were retained (so that the capillary term in (2.15*a*) is $\frac{1}{3}\overline{\partial}_x\{h^3[(\mathscr{S}+\epsilon^2\sigma)\,\overline{\partial}_x(h_x)]_x\}$ for example) have exhibited additional capillary waves where the film is thinnest.

reports of rupture by Fraaije & Cazabat (1989), who dropped oil onto water to measure its spreading rate (there were no Marangoni effects in this experiment). Clearly further studies, both theoretical and experimental, are necessary in order to establish the conditions that will result in rupture.

With much thinner liquid films in lung airways and alveoli, gravity becomes insignificant and diffusion more important. $\mathscr{D}$ remains sufficiently small for the similarity spreading rates of §3 to be potentially useful, however, in describing the behaviour either of an aerosol droplet landing on an alveolar wall, or of a planar front advancing along an airway. (In both cases the influence of the curvature of the underlying wall is small, and does not affect the overall spreading rates (Espinosa 1991).) If the liquid lining of an alveolus is as thin as 1 μm, for example, so that $\mathscr{D} = O(10^{-4})$ according to the parameter values given above, a period of $O(10^5$ s) is predicted to elapse before diffusion controls the spreading rate of a droplet; the dimensional droplet radius over this period is predicted by (3.11*b*) to be

$$\left(\frac{16}{\pi}\left(\frac{\mathrm{d}\sigma}{\mathrm{d}\Gamma}\right)^* M^* \frac{\tilde{H}}{\mu} t^*\right)^{\frac{1}{4}}, \tag{8.1}$$

where M^* is the dimensional equivalent of (3.1*b*), $(\mathrm{d}\sigma/\mathrm{d}\Gamma)^*$ the dimensional 'activity' of the surfactant at very weak concentrations and t^* the dimensional time. Natural lung surfactant can be expected to be present in the undisturbed lung liquid, however, and it is only if the concentration of this surfactant is sufficiently small ($\Gamma_\infty \ll 1$) that (8.1) is valid (Appendix A); furthermore, since one can expect Γ_∞ to exceed $\mathscr{D}$, it will be the disappearance of the surfactant gradient, rather than diffusion, that halts the spreading. Obviously many other effects will be important during the spreading process, particularly those related to the stability and solubility of the surfactant monolayer. In discussing a planar front we have so far assumed that surfactant is supplied to it at a rate of $t^{\frac{1}{3}}$: we cannot be certain that this is the appropriate condition for a front spreading along an airway. An important but still undetermined issue, relevant both to droplet and frontal spreading, is the rate at which surfactant is supplied to a monolayer from an attached bulk surfactant droplet at the critical micelle concentration.

In the thin liquid layers of the lung, the size of van der Waals interactions is considerably greater than in experiment, so that $\mathscr{A}$ and $\mathscr{S}$ are much closer in magnitude. There are no stabilizing gravitational forces, and diffusive effects are weak. Large film deformations can therefore be anticipated, and although the results of §7 do not predict that rupture instabilities should be likely with $\mathscr{A}$ two orders of magnitude smaller that $\mathscr{S}$, the experimental evidence of GG2 suggests that initial aerosol droplet–film interactions may very well induce film rupture. The consequences of rupture are potentially severe, since spreading of much of the droplet is halted, hindering effective therapy and possibly leaving patches of epithelium denuded. Factors making rupture less likely are therefore of therapeutic importance and include, for example, an increase in the surface diffusivity, or a reduction in the initial surfactant gradients, e.g. by a decrease in the concentration of surfactant in aerosol droplets, particularly when surfactant concentrations in the substrate are low.

This work was supported by NIH grants K04-HL01818, R01-HL41126 and NSF grant CTS-9013083.

Appendix A. Surface contamination of the undisturbed film

The two mutually dependent features sustaining the shock at the leading edge of a spreading surfactant monolayer are (i) that there is no surfactant on the undisturbed film ahead of the shock and (ii) that there is no transport of surfactant into the region ahead of the shock, implying that the surface velocity just behind the shock equals the shock speed. The balance between these two conditions is destroyed if there is surfactant on the film ahead of the shock (as is almost guaranteed to be the case in the lung, for example), and if it is assumed that the surfactant distribution is everywhere continuous, the shock solutions of §3 do not exist. Nevertheless, we can take advantage of the existing shock solutions by considering the effect of a very weak, uniform concentration of surfactant ($\Gamma_\infty \ll 1$) on the undisturbed film. Only the structure of the shock will be altered, while the outer solution behind it, and thus the shock speed, will remain unaffected. (It is worth noting that as a result the presence of very weak contamination will not influence the rupture instability described in §7.2.)

The inner solution in the frame of the shock is scaled by (5.1). We are interested in the situation in which $\Gamma(x,t) = \Gamma_\infty$ ahead of the shock, i.e. $Xt^{-(a+b)}G \to \Gamma_\infty$ as $\hat{\zeta} \to \infty$. Thus the lengthscale over which the shock adjusts to this downstream condition is $X_\infty = \Gamma_\infty t^{a+b}$. X_∞ grows at the same rate as $X_{\mathscr{D}}$ and $X_{\mathscr{G}}$ (see (5.3)), and will therefore be the dominant mechanism by which the shock is smoothed if $\Gamma_\infty \gg \mathscr{D}$ and $\Gamma_\infty \gg \mathscr{G}$. Let us suppose that this is the case. Then, letting $\zeta = \hat{\zeta} a \xi_s$ as before, and ignoring capillary effects (which will be important only at sufficiently early times), (5.2) becomes

$$H_\zeta + \tfrac{1}{2}(H^2 G_\zeta)_\zeta = 0, \quad G_\zeta + (HGG_\zeta)_\zeta = 0. \tag{A 1}$$

The corresponding boundary conditions resemble (5.6), except that $G \to 1$ as $\zeta \to \infty$. The appropriate solution of (A 1) is

$$H = \frac{2G}{G+1}, \quad \log\left(\frac{G+1}{G-1}\right) - 2G = \zeta. \tag{A 2}$$

Apart from the difference in the downstream boundary condition the shock structure resembles that shown in figure 5, with exponential decay downstream and algebraic decay upstream.

The lifetime of the shock in the presence of existing surfactant on the film is in general finite. For a strip or a drop, for example, the surfactant concentration in the advancing monolayer decreases as t^{-b}. Clearly once this falls to $O(\Gamma_\infty)$, the gradient driving the flow will no longer exist and the spreading will cease. This occurs after a time $\Gamma_\infty^{-1/b}$, which corresponds to the time at which $x_s \sim X_\infty$. Since $b = 0$ in the planar front case, however, spreading will persist indefinitely with the shock structure given by (A 2).

Appendix B. Additional singular effects

To complete the discussion of shock asymptotics we consider three additional effects that have so far been neglected from our model because they arose at $O(\epsilon^2)$ in the original formulation of the problem (§2; BG; GG1). Although they are unimportant throughout the majority of the flow, they have the potential to play significant roles in determining the structure of the shock because they act as singular perturbations. Our aim is primarily to determine the regions of parameter space, and the corresponding timescales, for which these effects may be important, and to indicate how they affect the shape of the shock.

B.1. *Surface viscosity*

If we assume that the boundary between substrate and gas, with or without a monolayer present, has the rheological properties of a Newtonian interface (Scriven 1960), the tangential stress condition at $z = h$ (2.11) should be written

$$u_z = \sigma_x + \epsilon^2 \bar{\partial}_x(\mathscr{K}(u_s)_x). \tag{B 1}$$

$\mathscr{K}$ is a non-dimensional surface dilational viscosity, given by $\mathscr{K} = k/\mu\tilde{H}$, where k is typically of the order 10^{-3}–10^{-1} g cm/s for most liquids (BG). $\mathscr{K}$ will be $O(1)$ or greater in sufficiently thin films, typically those for which $\tilde{H} \ll 1$ mm. Since surface viscosity will be significant only in the vicinity of the shock, where the variation in Γ is small, we are justified here in regarding $\mathscr{K}$ as independent of surfactant concentration, and thus of x, in (B 1).

For simplicity we neglect diffusive, capillary and gravitational effects, and again consider a linear equation of state. The horizontal velocity field (2.14) then becomes $u(x, z, t) = f(x, t)z$, where from (B 1)

$$f = -\Gamma_x + \epsilon^2 \mathscr{K} \bar{\partial}_x[(fh)_x], \tag{B 2}$$

and the governing equations (2.15) become

$$h_t + \tfrac{1}{2}\bar{\partial}_x(fh^2) = 0, \quad \Gamma_t + \bar{\partial}_x(\Gamma f h) = 0. \tag{B 3}$$

Away from the shock, $f = -\Gamma_x$ and (B 3) reduces to (3.3). Moving to the frame of the shock using the scalings of (5.1), assuming in addition that $f(x, t) = F(\hat{\zeta}, T)/t^{a+b}$, (B 2) transforms to

$$F = -G_{\hat{\zeta}} + \frac{\epsilon^2 \mathscr{K}}{X^2}(FH)_{\hat{\zeta}\hat{\zeta}}, \tag{B 4}$$

indicating that the lengthscale over which surface viscosity balances bulk viscosity and Marangoni forces is independent of time and is given by $X_{\mathscr{K}} = \epsilon \mathscr{K}^{\frac{1}{2}}$. Setting $X = X_{\mathscr{K}}$, expanding (B 3) in the frame of the shock and rescaling F and G by a factor $a\xi_s$ gives

$$H(1 - \tfrac{1}{2}FH) = 1, \quad G(1 - FH) = 0, \quad F = -G_{\hat{\zeta}} + (FH)_{\hat{\zeta}\hat{\zeta}}. \tag{B 5}$$

(B 5) has solutions $H = 2$, $G = -\frac{1}{2}\hat{\zeta}$, $F = \frac{1}{2}$ in $\hat{\zeta} < 0$ and, for $\hat{\zeta} > 0$, $H = (1 - (1 - 2F)^{\frac{1}{2}})/F$, $G = 0$ and

$$F = -((1 - 2F)^{\frac{1}{2}})_{\hat{\zeta}\hat{\zeta}}. \tag{B 6}$$

(B 6) has no exact solution, but since $0 \leqslant F \leqslant \frac{1}{2}$ a good approximation is obtained simply by considering a Taylor series expansion about $F = 0$. This gives $F = F_{\hat{\zeta}\hat{\zeta}} + O(F^2)$, so F and H decrease approximately exponentially in $\zeta > 0$ (F falls from $\frac{1}{2}$ to 0, H from 2 to 1). We see then that by opposing stretching of the interface, surface viscosity influences the film shape over a lengthscale $O(X_{\mathscr{K}})$, but has no effect on the surfactant distribution at the shock.

$X_{\mathscr{K}}$ decreases with respect to the length of the monolayer as time increases, and will therefore be of diminishing importance. In thin films (e.g. $\tilde{H} \ll 1$ mm) in which $\mathscr{K}$ is $O(1)$ or larger, gravitational effects will be negligible, so it will be either diffusion or capillarity that swamp the effects of surface viscosity. Since the capillary lengthscale $X_{\mathscr{S}}$ is generally larger at early times, this is the most likely to first exceed $X_{\mathscr{K}}$. With $\sigma_m/\tilde{S} = O(1)$, as is often the case, $\mathscr{S} = O(\epsilon^2)$, so that $X_{\mathscr{S}} \ll X_{\mathscr{K}}$ for $T \ll (\epsilon \mathscr{K}^{\frac{3}{2}})^{1/(a+b)}$. However, since $\mathscr{D}$ increases as $\tilde{H}$ falls, diffusion may be the first to dominate; $X_{\mathscr{D}} \ll X_{\mathscr{K}}$ for $T \ll (\epsilon \mathscr{K}^{\frac{1}{2}}/\mathscr{D})^{1/(a+b)}$. Thus it is only if

$$\mathscr{K} \gg \max(\epsilon^{-\frac{2}{3}}, (\mathscr{D}/\epsilon)^2) \tag{B 7}$$

that a significant period can exist in which the effects of surface viscosity will be evident.

B.2. *Stretching of the interface*

One term that was neglected from the surfactant conservation relation (2.12) is that describing how Γ is affected by stretching of the air–liquid interface (Scriven 1960; Stone 1989). Restoring this term, (2.12) becomes

$$\Gamma_t + \bar{\partial}_x(u_s\Gamma) + \epsilon^2\bar{\partial}_x(h_x)\,\Gamma(w - h_x u) = \mathscr{D}\bar{\partial}_x(\Gamma_x). \tag{B 8}$$

$\bar{\partial}_x(h_x)$ is the leading-order approximation to the curvature of the interface, and $w - h_x u$ approximates the velocity normal to the interface. As before, this effect is negligible throughout most of the flow, and the outer (similarity) solutions of §3 are unaffected by it, but it is a singular perturbation at the shock, so we should establish its importance.

Again, we choose to neglect the effects of diffusion, capillarity and gravity, so that the velocity fields are given by $u = \sigma_x z$ and $w = -\frac{1}{2}\sigma_{xx} z^2$. Moving to the frame of the shock using (5.1), (B 8) becomes, to leading order,

$$a\xi_s G_{\hat{\zeta}} + (GG_{\hat{\zeta}}H)_{\hat{\zeta}} + \left(\frac{\epsilon^2 T^{a+b}}{X^3}\right) H_{\hat{\zeta}\hat{\zeta}}(\tfrac{1}{2}H^2 G_{\hat{\zeta}})_{\hat{\zeta}} = 0. \tag{B 9}$$

Thus the lengthscale over which this stretching term acts is of size

$$X_{\text{stretch}} = (\epsilon^2 T^{a+b})^{\frac{1}{3}}. \tag{B 10}$$

Setting $X = X_{\text{stretch}}(a\xi_s)^{\frac{2}{3}}$ and $\zeta = a\xi_s\hat{\zeta}$, (B 9) may be integrated once, and with the rescaled H-evolution equation, $H(1 + \frac{1}{2}HG_\zeta) = 1$ (from (5.7*a*)), one obtains

$$H_\zeta = -\left(\frac{2G(2-H)}{H}\right)^{\frac{1}{2}}, \quad G_\zeta = \frac{-2(H-1)}{H^2}. \tag{B 11}$$

Examination of the (H, G)-phase space shows that there is a unique trajectory governed by (B 11) that satisfies (5.6*b*) and intersects the fixed point $(1, 0)$. The solution corresponding to this trajectory roughly resembles that shown in figure 5. For $\zeta > 0$, $H = 1$ and $G = 0$; as $\zeta \to 0-$, i.e. as the trajectory approaches the fixed point, $H \sim 1 - \frac{1}{9}\zeta^3$ and $G \sim \frac{1}{18}\zeta^4$. The stretching term therefore smoothes both the film height and the surfactant distribution, although it does not extend the length of the monolayer. The shock discontinuities arise in $H_{\zeta\zeta\zeta}$ and $G_{\zeta\zeta\zeta\zeta}$.

X_{stretch}, the lengthscale over which this term is effective, grows at exactly the same rate as the capillary lengthscale $X_{\mathscr{S}}$ ((5.3), B 11). Since $\mathscr{S} = O(\epsilon^2)$ in general, its effect will be coupled with capillarity, modifying the solution in §5.3. If $\mathscr{S}$ is $o(\epsilon^2)$, however, this term will be dominant at early times, before either diffusion or gravity control the flow at the shock.

B.3. *Inertia*

Very large spatial velocity gradients exist at the shock, making it likely that inertia influences the flow there. To investigate this possibility, we restore the inertial terms to the momentum equations (2.5), (2.6):

$$\epsilon^2 Re(u_t + uu_x + wu_z) = -p_x + u_{zz} + O(\epsilon^2), \tag{B 12a}$$

$$\epsilon^4 Re(w_t + uw_x + ww_z) = -p_z - \mathscr{G} + O(\epsilon^2). \tag{B 12b}$$

In order to re-express (B 12) using the scalings (5.1), ignoring for the moment any capillary, gravitational or diffusive effects, it is convenient to introduce a stream

function $\psi(x,z)$, which we write as $\psi = \Psi(\hat{\xi},z)/t^{a+b}$ to be consistent with (5.1). The sizes of the inertial terms in (B 12a) can then be compared to the $O(1)$ viscous term u_{zz}: the dominant inertial contribution comes from the convective terms $uu_x + wu_z$, which are $O(\epsilon^2 Re/Xt^{a+b})$. The inertial lengthscale is therefore

$$X_{Re} = \frac{\epsilon^2 Re}{t^{a+b}}. \tag{B 13}$$

As the shock advances it slows, and so inertial effects diminish in importance, at a rate greater than any others so far considered. Thus even with $Re = O(1)$, inertia will be significant only extremely early in the spreading process, during times in which both lubrication theory, and this asymptotic approximation, are unlikely to be valid.

REFERENCES

AHMAD, J. & HANSEN, R. S. 1972 A simple quantitative treatment of the spreading of monolayers on thin liquid films. *J. Colloid Interface Sci.* **38**, 601–604.

BORGAS, M. S. & GROTBERG, J. B. 1988 Monolayer flow on a thin film. *J. Fluid Mech.* **193**, 151–170 (herein called BG).

BRETHERTON, F. P. 1961 The motion of long bubbles in tubes. *J. Fluid Mech.* **10**, 166–188.

DIPIETRO, N. D., HUH, C. & COX, R. G. 1978 The hydrodynamics of the spreading of one liquid on the surface of another. *J. Fluid Mech.* **84**, 529–549.

ESPINOSA, F. F. 1991 Spreading of surfactant in a small pulmonary airway. MS thesis, Massachusetts Institute of Technology.

FRAALJE, J. G. E. M. & CAZABAT, A. M. 1989 Dynamics of spreading on a liquid substrate. *J. Colloid Interface Sci.* **133**, 452–460.

GAVER, D. P. III & GROTBERG, J. B. 1990 The dynamics of a localized surfactant on a thin film. *J. Fluid Mech.* **213**, 127–148 (herein called GG1).

GAVER, D. P. III & GROTBERG, J. B. 1992 Droplet spreading on a thin viscous film. *J. Fluid Mech.* **235**, 399–414 (herein called GG2).

HALPERN, D. & GROTBERG, J. B. 1992 Dynamics and transport of a localized soluble surfactant on a thin film. *J. Fluid Mech.* **237**, 1–11.

ROBERTSON, B. 1984 Pathology and pathophysiology of neonatal surfactant deficiency ('Respiratory Distress Syndrome', 'Hyaline Membrane Disease'). In *Pulmonary Surfactant* (ed. B. Robertson, L. M. G. van Golde & J. J. Batenburg) Elsevier.

RUCKENSTEIN, E. & JAIN, R. K. 1974 Spontaneous rupture of thin liquid films. *Chem. Soc. Faraday Trans.* 2 **70**, 132–147.

SCRIVEN, L. E. 1960 Dynamics of a fluid interface: equation of motion for Newtonian surface fluids. *Chem. Engng Sci.* **12**, 98–108.

SHAPIRO, D. L. 1989 Development of surfactant replacement therapy. In *Surfactant Replacement Therapy* (ed. D. L. Shapiro & R. H. Notter) New York: A. R. Liss.

SHARMA, A. & RUCKENSTEIN, E. 1986 An analytical nonlinear theory of thin film rupture and its application to wetting films. *J. Colloid Interface Sci.* **113**, 456–479.

STONE, H. A. 1989 A simple derivation of the time-dependent convective-diffusion equation for surfactant transport along a deforming interface. *Phys. Fluids* A **2**, 111–112.

TROIAN, S. M., HERBOLZHEIMER, E. & SAFRAN, S. A. 1990 Model for the fingering instability of spreading surfactant drops. *Phys. Rev. Lett.* **65**, 333–336.

TROIAN, S. M., WU, X. L. & SAFRAN, S. A. 1989 Fingering instability in thin wetting films. *Phys. Rev. Lett.* **62**, 1496–1499.

WILLIAMS, M. B. & DAVIS, S. H. 1982 Nonlinear theory of film rupture. *J. Colloid Interface Sci.* **90**, 220–228.